Atomistic Modeling of Quaternary Alloys: Ti and Cu in NiAl

GUILLERMO BOZZOLO, HUGO O. MOSCA, ALLEN W. WILSON, RONALD D. NOEBE, and JORGE E. GARCES

The change in site preference in NiAl(Ti,Cu) alloys with concentration is examined experimentally *via* ALCHEMI and theoretically using the Bozzolo–Ferrante–Smith (BFS) method for alloys. Results for the site occupancy of Ti and Cu additions as a function of concentration are determined experimentally for five alloys. These results are reproduced with large-scale BFS–based Monte Carlo atomistic simulations. The original set of five alloys is extended to 25 concentrations, which are modeled by means of the BFS method for alloys, showing in more detail the compositional range over which major changes in behavior occur. A simple but powerful approach based on the definition of atomic local environments also is introduced to describe energetically the interactions between the various elements and therefore to explain the observed behavior.

I. INTRODUCTION

THE influence of ternary alloying additions on the structure of binary ordered alloys is an area in which theory and experiment have kept pace with each other. Experimental techniques provide accurate and detailed data that are rather easily matched by current theoretical methods. Abundant work in this area has resulted in a thorough understanding of site occupancy and the underlying phenomena affecting the structure of materials. In spite of this promising starting point, severe limitations are almost immediately found if similar information is needed from more complex systems. That is definitely the case for the analysis of several minority elements in an otherwise simple (*i.e.*, binary) ordered alloy. It is only recently that some progress has been made in such analysis, at a fundamental level, due to the emergence of more accurate experimental techniques or, in the case of theoretical work, more computer power to attack complex problems.[1–4] Quantum approximate methods offer a new tool for investigating such problems by introducing simple formulations that translate into computationally efficient calculations.

In this article, we move one step forward, both theoretically and experimentally, in understanding the role of simultaneous alloying additions by studying a quaternary system, a NiAl-based alloy with Ti and Cu alloying additions. It is obvious that as the number of elements increases, the amount of available experimental evidence decreases, thus assigning modeling techniques a growing role in filling the gaps in our knowledge. The purpose of this work is to highlight this point, by presenting recent experimental work, using Atom Location by Channelling Enhanced Microanalysis (ALCHEMI)[5] on NiAl(Ti,Cu) alloys.[6] The experimental data were used to verify the modeling results and to validate the quantum approximate method used, the Bozzolo–Ferrante–Smith (BFS) method for alloys.[7] Once the modeling approach was validated, it was extended to a much broader set of compositions. We conclude with an analysis of the energetics of the system for a wide range of concentrations, including those studied experimentally. In doing so, we attempt to show how powerful modeling techniques supplement necessarily limited experimental data while at the same time providing global explanations of the observed behavior. To this end, this article is organized as follows. Section II describes the ALCHEMI results for five B2-structured NiAl(Ti,Cu) alloys ($Ni_{50}Al_{(47-x)}Ti_3Cu_X$, with $X = 1$, 3, and 6, and $Ni_{(50-x)}Al_{47}Ti_3Cu_X$, with $X = 1$ and 3), as shown in Figure 1. The site preference behavior of the Ti and Cu alloying additions as a function of Ni and Al concentration was determined. Section III describes the modeling effort, starting with the presentation of the results of Monte Carlo–Metropolis large scale atomistic simulations of those five experimental alloys, thus validating the use of the BFS method for alloys in this particular system. The modeling effort is then expanded to include detailed analytical BFS calculations for a wider range of concentrations, in order to provide much needed detail on the energetics and the resulting structure of the ground states. This is followed, in Section IV, with the introduction of a simple approach based on the BFS analysis for describing the energetics of the local atomic environments of the substitutional defects. Conclusions are drawn in Section V.

II. ALCHEMI ANALYSIS OF NiAl(Ti,Cu) ALLOYS

A. *Experimental Procedure*

The alloys in this study were created as variations of the base composition $Ni_{50}Al_{47}Ti_3$ (at. pct), as shown in Figure 1. In alloys 1 through 3, the amount of Al replaced by Cu was 1, 3, and 6 at. pct, respectively. Alloys 4 and 5 contain 1 and 3 at. pct Cu, respectively, added to replace Ni. The alloys were given a heat treatment consisting of a final homogenization treatment of 32 hours at 1644 K and aged for 6 hours at 1255 K, followed by air cooling. Transmission electron microscope (TEM) samples were prepared from 3-mm disks mechanically ground to 250 μm thickness. The ground disks were electropolished using a solution of 70 pct

GUILLERMO BOZZOLO, Senior Researcher, is with the Ohio Aerospace Institute, Cleveland, OH 44142. Contact e-mail: Guillermo.h.bozzolo@grc.nasa.gov HUGO O. MOSCA, Researcher, is with the Comision Nacional de Energía Atómica, 1063 Buenos Aires, Argentina. ALLEN W. WILSON, Staff Engineer, is with Boeing, Los Angeles, CA 90009. RONALD D. NOEBE, Materials Engineer, is with NASA Glenn Research Center, Cleveland, OH 44135. JORGE E. GARCES, Researcher, is with Centro Atomico Bariloche, 8400 Bariloche, Argentina.

Manuscript submitted May 25, 2001.

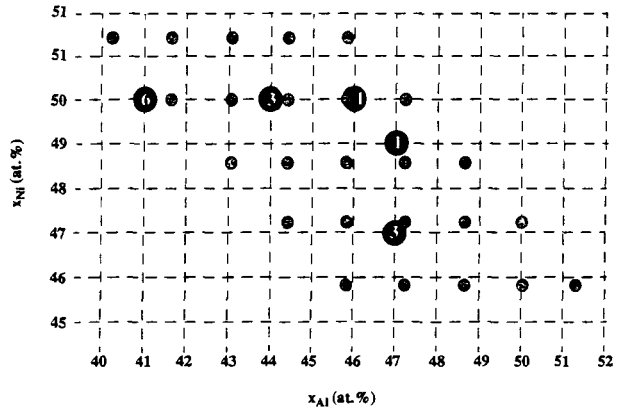

Fig. 1—Composition of the NiAl-Ti-Cu alloys modeled. Those for which experimental data exist[5] are denoted with filled circles. The numbers inside the circles indicate the concentration of Cu (in at. pct). The horizontal and vertical axes indicate the concentration of Al and Ni, respectively. The Ti concentration was held constant at 3 pct. The solid circles denote the alloys studied analytically with BFS.

ethanol, 14 pct distilled water, 10 pct butylcellosolve, and 6 pct perchloric acid at 20 V and 258 K. Energy-dispersive X-ray spectroscopy (EDS) was performed on a JEOL*

*JEOL is a trademark of Japan Electron Optics Ltd., Tokyo.

2010F TEM operating at 200 kV. The X-ray spectra were acquired and analyzed using a NIST Desktop Spectrum Analyzer (DTSA version 2.5.1). A cold stage specimen holder was used to minimize thermal vibrations, which may reduce the electron channeling required for the analysis. An area approximately 200 nm in diameter and 150-nm thick was used for the analyses with a beam convergence angle of 3.5 mrad.

B. *Electron Channelling–Enhanced Microanalysis*

The site occupancies were determined using the TEM–EDS technique of ALCHEMI.[5] This technique requires the acquisition of EDS spectra under carefully controlled dynamical electron diffracting conditions in a crystal. In the case of B2-ordered NiAl, an optimum condition occurs in a two-beam diffracting condition near $g = \langle 100 \rangle$.[5] By altering the diffraction conditions, the electron intensity along compositionally distinct planes can be controlled. This effect can be observed by acquiring EDS spectra at several diffracting conditions and measuring the relative changes in X-ray intensity for Ni and Al. If Ti or Cu is situated predominantly on one type of lattice site (either Ni or Al), its X-ray intensity will be altered in a like manner to the host element as diffracting conditions change. To explicitly calculate site occupancies, the diffraction-induced changes in generated X-ray intensities must be directly connected between alloying elements and host elements. Several methods of calculating site occupancies have been published in the literature.[8–12] In this analysis, the equations in Reference 13, described subsequently, were used to calculate the percentage of Ti and Cu on Al and Ni sites. In the case of Ti, X-ray generation is related to Ni and Al intensity by

$$I_{Ti} = \alpha_{Ni} I_{Ni} + \alpha_{Al} I_{Al} + C_{Ti} \qquad [1]$$

where I_x is the measured X-ray intensity of element x. The coefficients α_{Al}, α_{Ni}, and C_{Ti} can be fit using multiple regression[15] by collecting a set of I_{Ti}, I_{Ni}, and I_{Al} values for several diffracting conditions. Once the coefficients in Eq. [1] have been determined, the relative amount of Ti on Ni and Al sites can be calculated. Following the procedure outlined in Reference 13, which assumes that dynamical correction factors are independent of diffracting conditions, and assuming that the only relevant dynamical correction is for Al-K, the relative amount of Ti on Ni sites, f_{Ni}, is given by

$$f_{Ni} = \alpha_{Ni} \frac{I_{Ni}^{kinematic}}{I_{Ti}^{kinematic}} \qquad [2]$$

and the amount on Al sites is

$$f_{Al} = \alpha_{Al} \frac{I_{Al}^{kinematic}}{I_{Ti}^{kinematic}} + \frac{C_{Ti}}{I_{Ti}^{kinematic}} \qquad [3]$$

By accounting for the effect of Al-K delocalization in this analysis, the results are slightly different than those presented previously,[6] where the second term is used to compensate for delocalization of generated X-rays. These values can be normalized under the assumption that Ti can only reside on Ni or Al atomic sites.

Errors in this method of site occupancy measurement can be attributed to several factors. Anti-site defects, where Ni atoms do not exclusively reside on Ni lattice sites, will directly affect the measured channeling effect. Delocalization, where characteristic X-ray generation is not completely limited to lattice points, reduces the channeling effect for lower energy X-rays.[14] Standard sources of errors associated with EDS microanalysis in the TEM must also be considered. The error in the site occupancy calculation for this analysis is limited to the variables in each equation. Most of the errors in the calculations were due to the uncertainties in the multiple regression coefficients; however, the statistical errors in the measured X-ray intensities were also included. Assuming all variables in Eqs. [2] and [3] are independent, the uncertainty in the site occupancies can be estimated by the following equations:

$$\sigma_{f_{Ni}} = f_{Ni} \sqrt{\frac{\sigma_{\alpha_{Ni}}^2}{\alpha_{Ni}^2} + \frac{1}{I_{Ni}^{kinematic}} + \frac{1}{I_{Ti}^{kinematic}}} \qquad [4]$$

and

$$\sigma_{f_{Al}} = f_{Al} \sqrt{\frac{(I_{Ni}^{kinematic}\, \sigma_{\alpha_{Al}})^2 + \alpha_{Al}^2 I_{Al}^{kinematic} + \sigma_{C_{Ti}}^2}{(\alpha_{Al} I_{Ni}^{kinematic} + C_{Ti})^2} + \frac{1}{I_{Ti}^{kinematic}}} \qquad [5]$$

C. *Experimental Results*

After collecting the EDS spectra from several diffracting conditions (including kinematic) for each alloy, the spectra were background subtracted and the intensities were measured for the Al-K, Ni K_α, Ti K_α, and Cu K_α peaks. To illustrate the channeling effect, two EDS spectra collected at different diffracting conditions from alloy 3 are displayed in Figure 2. The spectra are normalized with respect to the Ni K_α peak. It is clear that the Al-K, Ti K_α and Cu K_α peaks are dramatically changed relative to the Ni K_α peaks. This initial examination of spectra indicates that the channeling

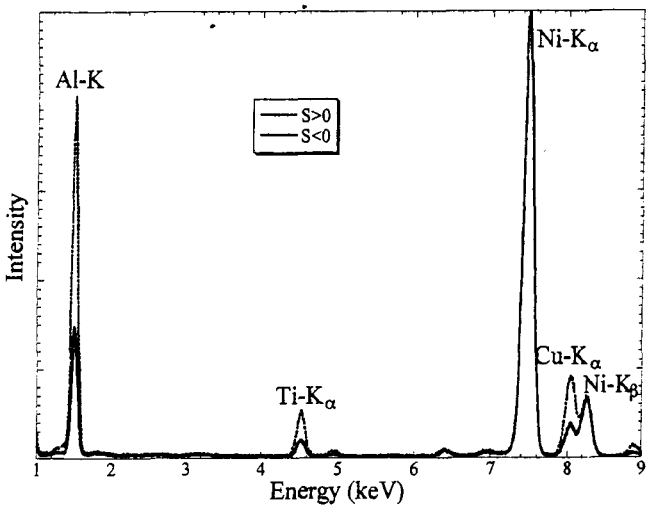

Fig. 2—EDS spectra from $Ni_{50}Al_{41}Ti_3Cu_6$ alloy at two strongly diffracting conditions near $g = \langle 100 \rangle$.

Table I. Percentage of Ti and Cu on Al Sites

Alloy	Ti	Cu
$Ni_{50}Al_{46}Ti_3Cu_1$	93.1 ± 5.2	77.1 ± 6.4
$Ni_{50}Al_{45}Ti_3Cu_2$	90.1 ± 10.0	91.8 ± 17.9
$Ni_{50}Al_{44}Ti_3Cu_3$	95.5 ± 8.0	88.1 ± 13.1
$Ni_{49}Al_{47}Ti_3Cu_1$	85.9 ± 6.4	29.6 ± 8.3
$Ni_{47}Al_{47}Ti_3Cu_3$	87.3 ± 15.9	6.8 ± 18.7

effect is strong, and both Ti and Cu preferentially reside on Al lattice sites in this alloy.

Similar analysis was performed on all five alloys and the site occupancies for Ti and Cu (Eqs. [2] and [3]) are listed in Table I, along with the calculated uncertainties. The results demonstrate that the Cu content on Al sites is strongly dependent upon the stoichiometry of the alloy, whereas the Ti strongly prefers Al sites for all alloys. A major portion of the uncertainties listed in Table I was due to statistical error in the C_{Ti} constant, which was included to incorporate a delocalization correction for the Al-K X-ray line (Eq. [3]). It also introduced a significant amount of error in the calculation. Nevertheless, the calculation indicates that Cu substitutes for either Ni or Al sites, depending on stoichiometry.

III. THEORY

A. *The BFS Method for Alloys*

The BFS method for alloys has been extensively used for the analysis of ordered intermetallic alloys due to its ability to describe multicomponent systems with the same simplicity and accuracy as binary systems.[7,16–18] Unlike other quantum approximate methods of similar computational characteristics, BFS benefits from its universal parameterization, which allows it to deal with NiAl, NiAlTi, NiAlCu, and NiAlTiCu alloys with the same set of parameters, regardless of concentration or composition, as long as we are dealing with a bcc-type structure, including B2, Heusler, and other bcc derivative compounds.

In this section, we provide a brief description of the operational equations of BFS. The reader is encouraged to seek further details in previous articles where a detailed presentation of the foundation of the method, its basis in perturbation theory, and a discussion of the approximations can be found.[7] The BFS method provides a simple algorithm for the calculation of the energy of formation of an arbitrary alloy (*i.e.*, the difference between the energy of the alloy and that of its individual constituents). In BFS, the energy of formation is written as the superposition of elemental contributions of all the atoms in the alloy:

$$\Delta H = \sum_i \varepsilon_i \qquad [6]$$

For each atom, we partition the energy ε_i into two parts: a strain energy and a chemical energy contribution. The BFS strain energy relates only to the atomic positions of the neighboring atoms to atom i, regardless of their chemical identity. For its calculation, we use the actual geometrical distribution of the atoms surrounding atom i, computed as if all of its neighbors were of the same species as atom i. Its calculation is then straightforward, even amenable to first-principles techniques. In our work, we use equivalent crystal theory (ECT)[19] for its computation, due to its proven ability to provide accurate and computationally economical answers to most general situations.

The chemical environment of atom i is considered in the BFS chemical energy contribution, where the surrounding atoms maintain their identity but are forced to occupy equilibrium lattice sites corresponding to the reference atom i. Building on the concepts of ECT, a straightforward approach for the calculation of the chemical energy is defined, properly parameterizing the interaction between dissimilar atoms.[7]

Thus defined, the BFS strain and chemical energy contributions take into account different effects, *i.e.*, geometry and composition, computing them as isolated behaviors. A coupling function, g_i, restores the relationship between the two terms, defined in such a way as to properly consider the asymptotic behavior of the chemical energy, where chemical effects are negligible for large separations between dissimilar atoms. The contribution by atom i to the energy of formation is then $\varepsilon_i = \varepsilon_i^S + g_i \varepsilon_i^C$. The strain energy contribution, ε_i^S, is obtained by solving the ECT perturbation equation:

$$NR_1^{P_i} e^{-\alpha_i R_1} + MR_2^{P_i} e^{-\left(\alpha_i + \frac{1}{\lambda_i}\right)R_2} = \sum_j r_j^{P_i} e^{-(\alpha_i + S(r_j))r_j} \qquad [7]$$

where N and M are the number of nearest-neighbors (NN) and next-nearest neighbors (NNN), respectively, and where p, l, α, and λ are ECT parameters that describe element i (Reference 19 provides definitions and details), r denotes the distance between the reference atom and its neighbors, $S(r)$ describes a screening function,[19] and the sum runs over NN and NNN. This equation determines the lattice parameter of a perfect equivalent crystal where the reference atom i has the same energy as it has in the geometrical environment of the alloy under study. The terms R_1 and R_2 denote the NN and NNN distances in this equivalent crystal. Once the lattice parameter of the (strain) equivalent crystal, a^S, is determined, the BFS strain energy contribution is computed using the universal binding energy relation of Rose *et al.*,[20] $\varepsilon_i^S = E_C^i(1 - (1 + a_i^{S*})e^{-a_i^{S*}})$, where E_C^i is the cohesive energy of atom i and where the scaled lattice parameter a_i^{S*} is given by $a_i^{S*} = (q/l_i)(a_i^{S*} - a_e^i)$, where q is the ratio

between the equilibrium Wigner–Seitz radius and the equilibrium lattice parameter a_e^i.

The BFS chemical energy, ε_i^C, is obtained by a similar procedure. The surrounding atoms retain their chemical identity, but are forced to be in equilibrium lattice sites of an otherwise monatomic crystal i. The BFS equation for the chemical energy is given by

$$NR_1^{P_i}e^{-\alpha_i R_1} + MR_2^{P_i}e^{-\left(\alpha_i-\frac{1}{\lambda_i}\right)R_2} = \sum_k \left(N_{ik}r_1^{P_i}e^{-\alpha_{ik}r_k} + M_{ik}r_2^{P_i}e^{-\left(\alpha_{ik}+\frac{1}{\lambda_i}\right)r_2}\right) \quad [8]$$

where N_{ik} and M_{ik} are the number of NN and NNN of species k of atom i. The chemical environment surrounding atom i is reflected in the parameters α_{ik}, given by $\alpha_{ik} = \alpha_i + \Delta_{ki}$, where the BFS parameters Δ (a perturbation on the single-element ECT parameter α_i) describe the changes of the wave function in the overlap region between atoms i and k. Once Eq. [8] is solved for the equivalent chemical lattice parameter a_i^C, the BFS chemical energy is then $\varepsilon_i^C = \gamma^i E_C^i(1 - (1 + a_i^{C*})e^{-a_i^{C*}})$, where $\gamma_i = 1$ if $a_i^{C*} > 0$ and $\gamma_i = -1$ if $a_i^{C*} < 0$. The scaled chemical lattice parameter is given by $a_i^{C*} = (q/l_i)(a_i^C - a_e^i)$. Finally, as mentioned previously, the BFS chemical and strain energy contributions are linked by a coupling function g_i, which describes the influence of the geometrical distribution of the surrounding atoms in relation to the chemical effects and is given by $g_i = \exp(-a_i^{S*})$. The pure element parameters a_e, E_c, l, α, and λ, computed using the linear-muffin-tin orbital method (LMTO)[21] in the atomic sphere approximation, and the BFS parameters, Δ_{AB} and Δ_{BA}, for A and B = Ni, Al, Ti, and Cu, used in this study are listed in Reference 17. These same parameters are used in any calculation involving these four elements, regardless of the type of defects present (including surfaces) and the composition of the alloy, as long as the final crystal structure remains bcc.

B. *BFS Modeling*

The first step in our modeling effort consists of testing the ability of the theoretical method to reproduce the experimental results. In this case, it is necessary to perform computer experiments for the same five concentrations studied *via* ALCHEMI, as shown in Figure 1. Clearly, no single theoretical technique can reproduce all the subtleties of an experiment, much less simultaneously deal with all the length and time scales involved. It is not strictly necessary, however, to perform a perfect theoretical simulation of the experiment. For the purpose of this work, it suffices to implement a ground state search where a large collection of atoms is allowed to evolve to its lowest energy state following a predetermined temperature-dependent process. This is best achieved by means of Monte Carlo–Metropolis simulations.[16] Due to the number of elements involved in these calculations, a full Monte Carlo treatment should include individual atomic relaxations and the ability of the system to evolve to a multiphase structure. However, previous work on the determination of the site occupancy of additions to NiAl[16,17,22] indicates that, for the range of concentrations studied, it suffices to consider only global relaxations, where only the lattice parameter of the alloy (*i.e.*, computational cell) is varied until the energy is minimized, thus introducing a substantial simplification in the calculations. It should be noted that in the absence of a satisfactory foundation for this approximation, a full treatment of relaxations must be performed.

1. *Large scale simulations*

Monte Carlo–Metropolis simulations using the BFS method are performed in a sufficiently large atom population (1024 atoms). In these simulations, pairs of atoms at NN distance are allowed to switch places with a probability exp $(-\Delta E/kT)$, where k is the Boltzmann's constant, T is the temperature, and ΔE is the difference in energy of the cell before and after the switch. The changes in atomic distribution are allowed to continue until the total energy of the cell stabilizes. Every computational cell has been subject to the same temperature treatment, where an initial random distribution of atoms is steadily cooled from over 2000 K to room temperature.

2. *Verification of Monte Carlo results with experiment*

The results for the five alloys that were studied experimentally[6] are shown in Figure 3. Besides the obvious insight that can be obtained from direct visual inspection, valuable information can also be extracted from the coordination matrix of the final, stable state for each cell, where the matrix element a_{mn} represents the probability that an atom m has an atom n as a NN.

Table II displays the coordination matrices for the five alloy concentrations studied. As long as the cell follows the basic B2 ordering (in this case, Ni and Al atoms occupying their own sublattices), then $a_{m\text{Ni}}$ and $a_{m\text{Al}}$ can be taken as an *approximate* measure of the likelihood that an atom m occupies a site in the Al or Ni sublattice, respectively. If $P[m(n)]$ denotes the probability of an atom m occupying a site in the n sublattice, then the previous statement can be written as $a_{m\text{Ni}} \sim P[m(\text{Al})]$ and $a_{m\text{Al}} \sim P[m(\text{Ni})]$. Large values of the diagonal elements in each matrix can indicate either antiphase boundaries or the presence of precipitates (*i.e.*, a large value of a_{NiNi} indicates that many Ni atoms are at NN distance, which would be highly unlikely in a NiAl alloy, where, if perfectly ordered, $a_{\text{NiNi}} = 0$). If the diagonal elements are small, then the off-diagonal elements can be taken as a good approximation of the site preference. In other words, if a_{NiNi} and a_{AlAl} are small, the closer the cell is to a highly ordered state, which translates into a_{TiNi} being a true measure of the likelihood of finding Ti in an Al site.

In agreement with experimental results and the conclusions reached in Reference 6, the simulations show that Cu does change site preference in NiAl, depending on the ratio of Ni to Al, as seen in the variations of a_{CuNi} in Table II. For the five alloys shown, $P[\text{Ti(Al)}] > P[\text{Ti(Ni)}]$, whereas $P[\text{Cu(Al)}] > P[\text{Cu(Ni)}]$ for Ni-rich alloys and $P[\text{Cu(Ni)}] > P[\text{Cu(Al)}]$ otherwise. Figure 3(f) shows a comparison of the computed site occupation probabilities $P[\text{Ti(Al)}]$ and $P[\text{Cu(Al)}]$ with those determined experimentally,[6] clearly showing the agreement between experiment and theory and providing a great degree of confidence in the BFS-based simulations.

The possibility of a general trend in site occupancy as a function of NiAl concentration warrants additional simulations for a range of concentrations that includes the five studied experimentally (Figure 1). Figure 4 shows $P[\text{Ti(Al)}]$ (Figure 4(a)) and $P[\text{Cu(Al)}]$ (Figure 4(b)) as a function of Al, Ni, and Cu concentration. As expected, $P[\text{Ti(Al)}]$ is

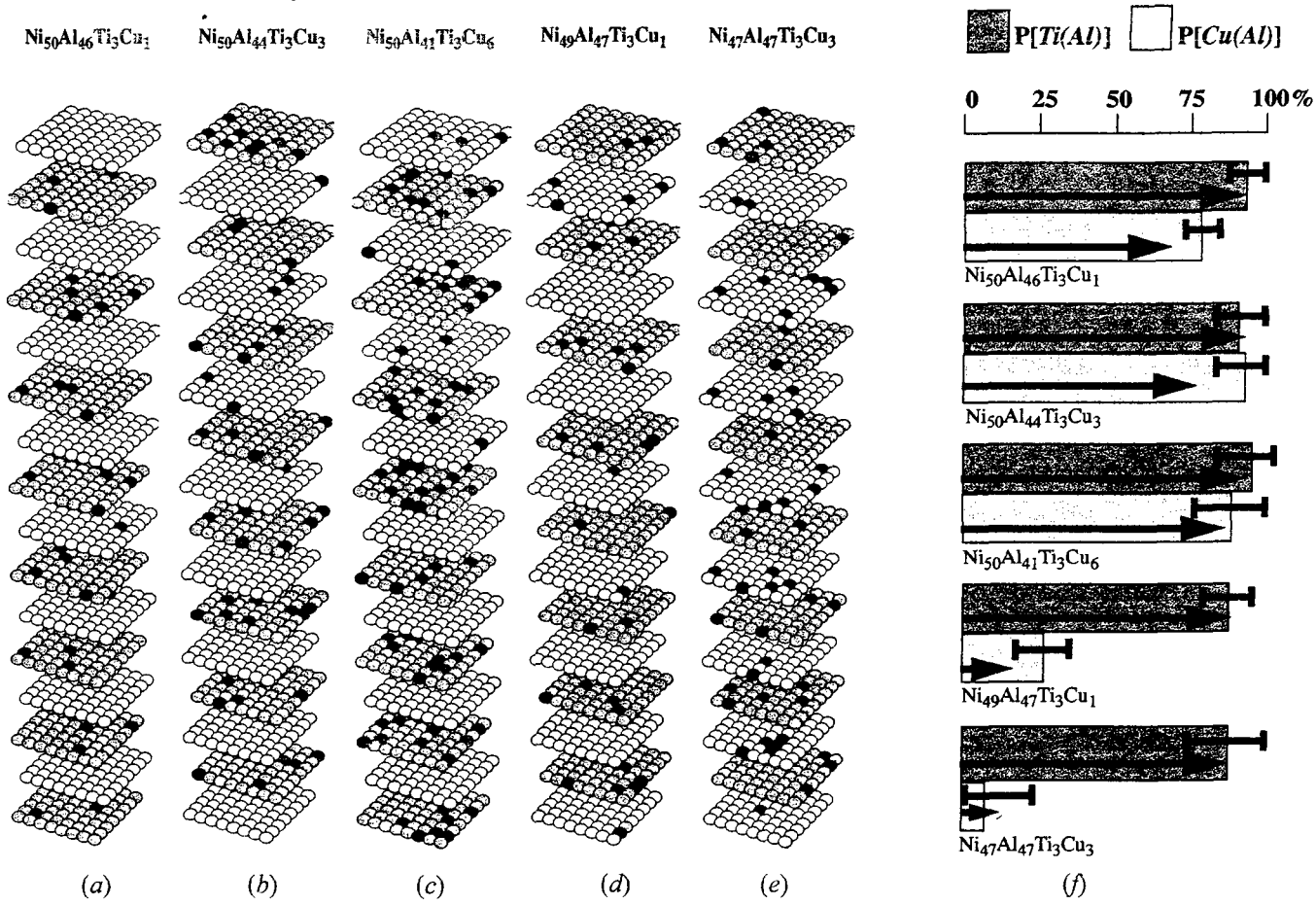

Fig. 3—(*a*) through (*e*) Final structures of the Monte Carlo/Metropolis/BFS simulations of the five alloys studied in Ref. 6. White, light gray, dark gray, and black spheres denote Ni, Al, Cu, and Ti atoms, respectively. The 1024 atom cells are stretched along the vertical axis to guide the eye. (*f*) Comparison of the occupation probabilities P[Ti(Al)] and P[Cu(Al)] from experiment (shaded rectangles), with the corresponding uncertainties. The BFS results are indicated with arrows.

always significantly greater than zero. The minimum value obtained is 54 pct for $Ni_{46}Al_{51}Ti_3$. In contrast, Cu(Al) decreases much more rapidly than Ti(Al) for increasing Al concentration and decreasing Ni and Cu concentration, eventually becoming zero. This behavior indicates a switch in site preference exclusively favoring Ni sites ($a_{CuNi} = 0$). This can also be seen in Figure 4(b), in the shape of a vaguely defined "boundary." This transitional regime, loosely defined by alloys with a 1:1 Ni:Al ratio, is a region where P[Cu(Al)] (or the matrix element a_{CuNi}) displays a sharp drop for decreasing Ni:Al ratios and where the corresponding Ti site preference for Al sites (P[Ti(Al)], or a_{TiNi}) in Figure 4(a) decreases at a much slower rate and is mostly independent of Cu concentration. In this sense, mapping of the simulated results indicates much greater sensitivity of P[Cu(Al)] with concentration than that seen for P[Ti(Al)]. While the experimental results suggest a sudden reversal in site preference for Cu at a specific stoichiometry, the theoretical results indicate that this is a more gradual change beginning for alloys with 1:1 Ni:Al ratio (*i.e.*, the "surface" that could be built from the data displayed in Figure 4 for either P[Ti(Al)] or P[Cu(Al)] would resemble a "cascade," smoothly evolving from one regime to another, as opposed to a sharp "step," where there is no transitional region). We can also draw some general conclusions regarding the interaction between Ti and Cu atoms in the NiAl matrix. While $a_{TiTi} = 0$ in every single alloy studied (indicating a strong repulsion between Ti atoms), a_{CuCu} is (in most cases) finite, allowing the possibility of clustering of a small fraction of Cu atoms, particularly for Ni-rich alloys (for example, $a_{CuCu} = 3.0$ for $Ni_{50}Al_{43}Ti_3Cu_4$, indicating that a Cu atom has a 3 pct probability of having another Cu atom as a NN). Moreover, the interaction matrix elements a_{TiCu} and a_{CuTi} are generally small for Ni-rich alloys, indicating the presence of few Ti and Cu NN pairs and, therefore, a higher likelihood of finding both elements in Al sites. These probabilities slowly increase as the concentration of Ni decreases, consistent with the fact that, for this range of concentrations, P[Cu(Al)] decreases much faster than P[Ti(Al)], thus favoring the location of Ti and Cu atoms in different sublattices. This results in a switch of site preference for Cu atoms from Al to Ni sites with a change in stoichiometry, as observed experimentally.

Summarizing the results from these simulations, the strong ordering tendencies of NiAl alloys, coupled with the strong preference of Ti for Al sites, as well as the less prominent interaction between Cu and Ti atoms and the small energy difference for Cu atoms in Ni *vs* Al sites, all contribute to make Cu atoms the ones most likely to fill in for any deficiency on either side of stoichiometry. This translates into

Table II. Coordination Matrices for the 5 NiAl-Ti-Cu Alloys Identified in Figure 1 and Displayed in Figure 3. Each Matrix Element a_{mn} is Related to the Probability (in Percent) That an Atom n Has an Atom m as a NN, $P[m(n)]$; for Example, the Probability That Ti has Ni as a NN, a_{TiNi}, for an Alloy of Composition $Ni_{50}Al_{41}Ti_3Cu_6$ is 98.4 Pct, Indicating That Ti Resides Almost Exclusively on the Al Sublattice

$m\backslash n$		Ni	Al	Ti	Cu
(a) $Ni_{50}Al_{41}Ti_3Cu_6$	Ni	4.3	80.2	6.0	6.6
	Al	97.7	0.	0.0	2.3
	Ti	98.4	0.0	0.0	1.6
	Cu	80.3	15.6	0.8	3.3
(b) $Ni_{50}Al_{44}Ti_3Cu_3$	Ni	2.7	86.6	6.0	4.7
	Al	98.5	0.0	0.0	1.5
	Ti	99.2	0.0	0.0	0.8
	Cu	77.0	21.4	0.8	0.8
(c) $Ni_{50}Al_{46}Ti_3Cu_1$	Ni	1.2	91.4	6.0	1.3
	Al	99.4	0.0	0.0	0.6
	Ti	99.6	0.0	0.0	0.4
	Cu	68.8	27.5	1.2	2.5
(d) $Ni_{49}Al_{47}Ti_3Cu_1$	Ni	0.0	93.7	6.1	0.2
	Al	97.8	0.3	0.0	1.8
	Ti	98.4	0.8	0.0	0.08
	Cu	10.0	87.5	2.5	0.0
(e) $Ni_{47}Al_{47}Ti_3Cu_3$	Ni	0.0	93.8	6.2	0.0
	Al	93.8	0.0	0.0	6.2
	Ti	96.4	0.0	0.0	3.6
	Cu	0.0	96.4	3.6	0.0

a smooth transition from Al to Ni site occupancy as the change in composition becomes Ni poor.

3. *BFS analytical calculations*

Large-scale simulations provide, at best, a theoretical confirmation of the experimental results and, through the coordination matrices, some general insight on the possible underlying trends. Monte Carlo simulations provide useful information regarding the most likely final state of a given system. However, BFS-based detailed analytical calculations can provide information on the structure of the low-lying energy states (*i.e.*, most likely to appear) and the energetics of individual atoms or groups of atoms. A large set of reasonably large atomic configurations, each displaying a different distribution of atoms in a given computational cell, is defined and its energy of formation computed using BFS. In this work, it proves to be sufficient to work on a 72-atom cell, as most relevant atomic distributions can be properly described. In what follows, we will use the notation $Ni_{[i]}Al_{[j]}Ti_{[k]}Cu_{[l]}$ to denote the concentration of the alloy in terms of the number of atoms in the 72-atom cell. Therefore, $[i] = 36$ corresponds to 50 at. pct Ni.

In order to match the compositions studied either experimentally or with Monte Carlo simulations as closely as possible, we define 25 compositions that properly cover the entire range of Ni, Al, and Cu concentrations studied before. These states, denoted with gray solid circles in Figure 1, correspond to alloys $Ni_{[A]}Al_{[B]}Ti_{[2]}Cu_{[C]}$, where the subindex indicates the number of atoms of each species in the 72-atom cell (A + B + C = 70). For each concentration, we build a catalogue of configurations that, if large enough, contains every possible arrangement of atoms that is likely to occur in the real alloy. We then compute the energy of formation of each cell and plot the results in the form of an energy level spectrum, where, for each concentration, we can understand what atomic configurations are energetically favored and which ones are not. The number and type of configurations included in each catalogue are, in principle, arbitrary. In this work, a total of 300 configurations were used (for the entire range of concentrations studied). Examples of configurations included in the catalogue are shown in Figure 5, where some selected configurations for one particular concentration, $Ni_{[36]}Al_{[30]}Ti_{[2]}Cu_{[4]}$, are shown. These cells can be described by labeling their differences with a basic B2 ordered NiAl cell. It is therefore convenient

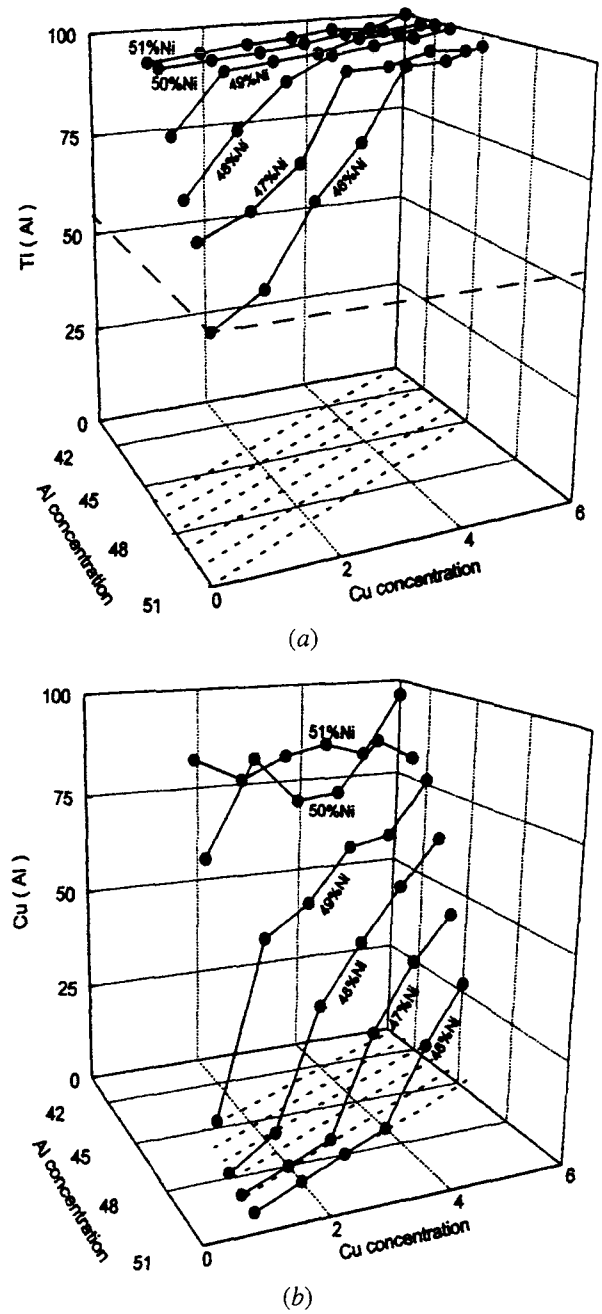

Fig. 4—Matrix elements (*a*) a_{TiNi} and (*b*) a_{CuNi}, taken as a measure of P[Ti(Al)] and P[Cu(Al)], respectively, as a function of Al and Cu concentration, for different values of x_{Ni}. The projection of these curves onto the horizontal plane is shown with dashed lines, highlighting the fact that Cu(Al) becomes zero for high Al concentration and low Ni and Cu concentration.

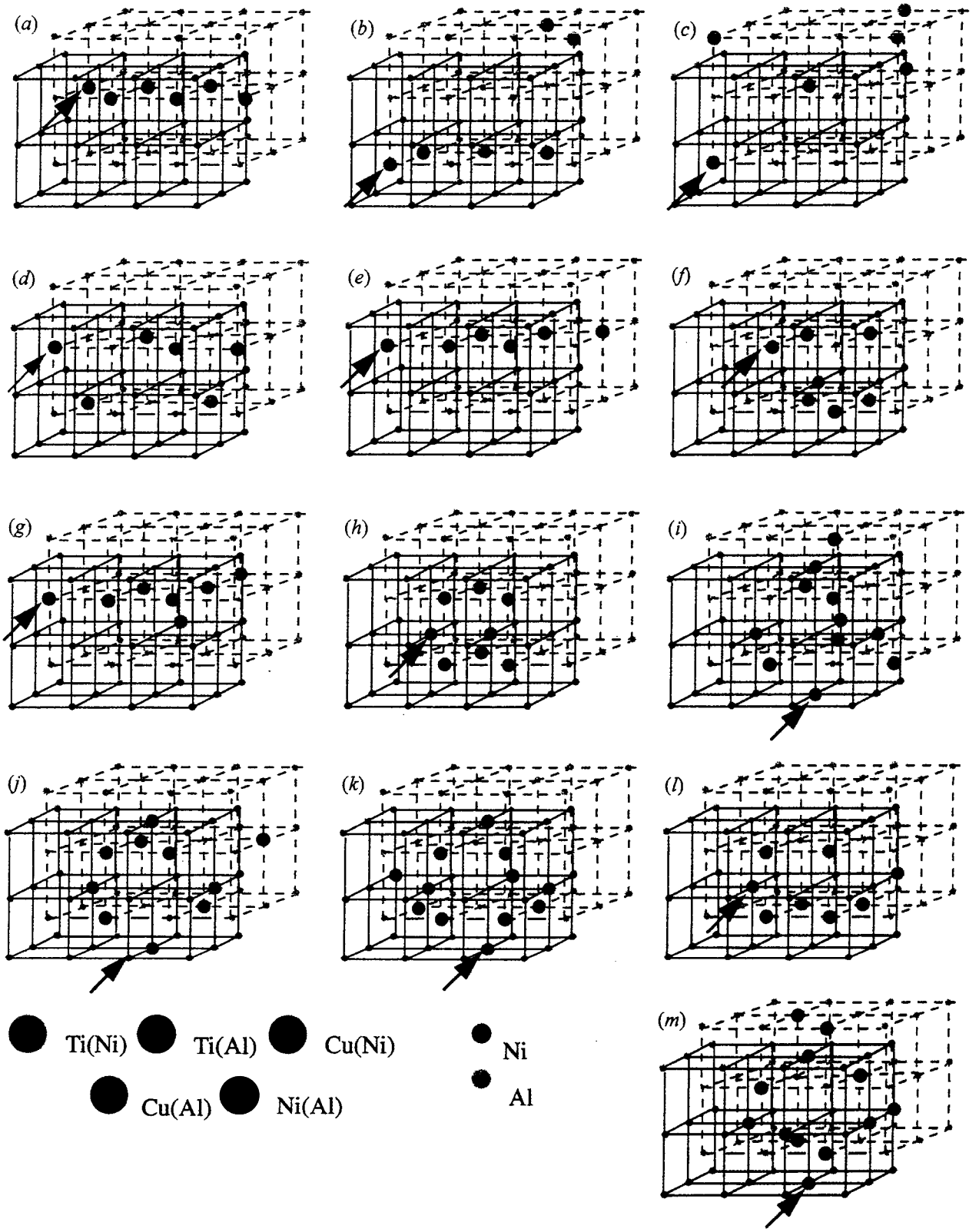

Fig. 5—(*a*) through (*m*) Some configurations for $Ni_{[36]}Al_{[30]}Ti_{[2]}Cu_{[4]}$. Based on a NiAl 72-atom cell where the Ni sublattice is denoted with solid lines and the Al sublattice with dashed lines, Ti additions are denoted with cyan (blue) disks if located in the Ni (Al) sublattice, and Cu additions are noted with magenta (red) disks if located in the Ni (Al) sublattice. Antistructure Ni atoms are denoted with large black disks. Otherwise, small black (gray) disks denote Ni (Al) atoms in their respective sites. The arrow indicates the first atom listed in the expressions displayed in Table III, where a general description of the chain of substitutional defects is provided.

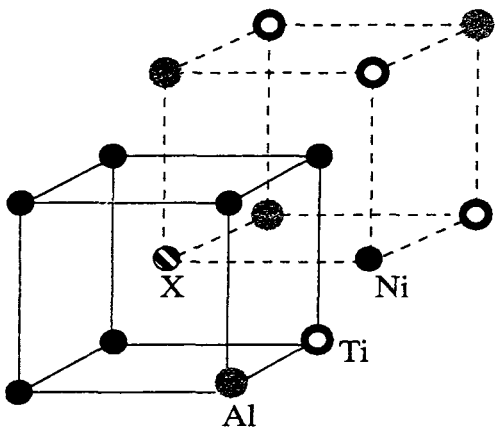

(b) $X(Ti)Ti(Ni)_1Ni(Al)_{1,2}Al(Ni)_{1,2,1}$

Ni Al Ti X

Fig. 6—A Ni_2AlTi cell after the introduction of an X atom in a Ti site (X(Ti)), the Ti atom moving to a Ni site (Ti(Ni)) so that the X and Ti atoms are located at NN distance, the Ni atom moving to an Al site (Ni(Al)) so that Ni is at NN distance with Ti and is a second neighbor of X, and the Al atom moving to a Ni site (Al(Ni)) so that it is NN of the Ni atom, second neighbor of the Ti atom and first neighbor of the X atom.

to describe the relative location of each atom in the sample by means of a simple notation, which, while by no means complete, provides a first glimpse at the structure of each cell. In what follows, A and B represent the two simple cubic sublattices of the B2 compound and X represents a ternary alloying addition. The term X(A) denotes an atom X substituting for an atom A on the A sublattice, and $X(A)A(B)_n$ denotes the same case but with the displaced A atom occupying a site in the B sublattice. The distance between atoms X and A is denoted by the subindex n. If $n = 1$, atoms X and A are NN, while $n = 2$ indicates NNN.

This notation can be easily generalized to describe more complex situations. In a chain of point defects, the first subindex denotes the distance (measured in NN or NNN distances) between the indexed defect and the one preceding it, and subsequent indices denote the separation of the labeled atom with previous atoms (from right to left) in the chain. For example, $X(A)A(B)_1B(A)_{1,2}$ indicates an X atom occupying an A site and the A atom in a B site, so that X and A are NN ($X(A)A(B)_1$). The B atom then moves to another A site, so that A and B are NN (the first subindex in $B(A)_{1,2}$) and B and X are NNN (the second subindex in $B(A)_{1,2}$). Due to the fact that, in this application of BFS we deal with, at most, NNN interactions, we will not specify the distance between point defects if it exceeds the NNN distance. As an example, Figure 6 shows a variation of the perfect Ni_2AlTi ($L1_2$) Heusler cell where a chain of point defects is generated by the introduction of an atom X in a Ti site. The Ti atom in that site moves to a neighboring Ni site and, in turn, the displaced Ni atom moves to an Al site and, finally, the Al atom moves to an available Ni site. The X and Ti atoms are located at NN distance, the Ni and Ti atoms are located at NN distance and the Ni and X atoms are at NNN distance. Finally, The Al atom is a NN of the Ni atom, a NNN of the Ti atom, and a NN of the X atom (subindices 1, 2, and 1, respectively). The series of defects then reads $X(Ti)Ti(Ni)_1Ni(Al)_{1,2}Al(Ni)_{1,2,1}$. In an expression dealing with several defects, the symbol $X(A)_{...,n}$ ($n = 1$ and 2) means that atom X is at NN ($n = 1$) or NNN ($n = 2$) distance from the first atom listed in the expression.

We now return to the sample catalogue shown in Figure 5 and write the corresponding series of substitutions using this notation in Table III. After minimizing the energy of formation of each cell with respect to the lattice parameter, we can order the configurations in an energy level spectrum, together with the resulting value of the lattice parameter, as shown in Table III. We also show the number and type of substitutional defects noting, not surprisingly, that the states with lower energy are those where Ti and Cu occupy Al sites.

4. *Ground state analysis*

Having shown the results for the ground state search for one specific concentration ($Ni_{[36]}Al_{[30]}Ti_{[2]}Cu_{[4]}$), we now repeat this procedure for all the remaining compositions noted in Figure 1 and determine, in each case, the ground state. First, we concentrate on the structure of the ground states as a function of Cu concentration. The strong site preference of Ti for Al sites guides this choice, as it allows for a clear understanding of the behavior of Cu as it increases its role in the system. A series of $Ni_{[38-x]}Al_{[32+x]}Ti_{[2]}$, ($x = 1, \ldots, 5$) alloys helps establish the behavior of Ti, when it is the only alloying addition. The behavior is dictated by the strong site preference of Ti for Al sites, regardless of the ratio between Ni and Al atoms. This preference for Al sites is absolute, in that Al antistructure atoms are created, if necessary, to accommodate all the Ti atoms in the Al sublattice (Ti(Al)), as shown in Figure 7. The Ti(Al) atoms, however, are somewhat sensitive to the presence of antisite defects, whether these are Ni atoms in the Al sublattice (which attract other Ti(Al) atoms at NNN distance) or Al atoms in the Ni sublattice (which attract Ti(Al) atoms at NN distance). The number of antistructure Al atoms is reflected in the rapidly increasing energy of formation for this set of alloys, with an average increase of 0.055 eV/atom per antisite defect. The actual atomic distribution in each alloy, as well as a simple schematic representation of these states highlighting the behavior of the added Ti atoms, is shown in Figure 7.

The $Ni_{[38-x]}Al_{[31+x]}Ti_{[2]}Cu_{[1]}$, ($x = 1, \ldots, 5$) alloys are shown in Figure 8, following the same format and notation used in Figure 7. This set of alloys shows the first indication of the interaction between Ti and Cu. Once again, Ti(Al) substitutions dominate, leaving Cu second choice for available Al sites. The Ti(Al) preference is strong enough as to induce the creation of Al antistructure atoms. Moreover, Ti(Al) seems to attract available Cu(Al) atoms along the [100] direction, thus inducing an ordered pattern where Ti and Cu atoms occupy alternating sites in the Al sublattice. However, the interaction between Ti(Al) and Cu atoms seems to be restricted to those cases where Cu goes to Al sites only. If Cu atoms are forced to go to Ni sites, they ignore the presence of Ti(Al) linking themselves only to Al antistructure atoms. These results highlight dominant (Ti(Al) inducing antistructure atoms) and secondary (Cu(Al) linked to Ti(Al)) features characterizing this group of alloys. So far, the main features that characterize the $N_{Cu} = 0$ and $N_{Cu} = 1$ cases are (1) absolute preference of Ti for Al sites; (2)

Table III. Description of the Cells Displayed in Figure 5 in Terms of the Different Substitutional Atoms, Relative to a Perfectly Ordered B2 NiAl Cell; the Number of Substitutional Atoms in Each Expression, the Difference in Energy of Formation (in eV/Atom) between the Cell and a Perfectly Ordered B2 NiAl Cell and the Value of the Lattice Parameter (in Angstroms) That Minimizes Such Difference Are Also Shown

Cell	Description	Ti(Al)	Ti(Ni)	Cu(Al)	Cu(Ni)	Ni(Al)	ΔH-ΔH_0	a
a	$Cu(Al) + Ti(Al)_2 + Cu(Al)_2 + Ti(Al)_2 + Cu(Al)_{2,f,2} + Cu(Al)_{f,2}$	2	0	4	0	0	0.04274	2.8448
b	$Cu(Al) + Ti(Al)_2 + Cu(Al)_2 + Ti(Al)_2 + Cu(Al)_2 + Cu(Al)$	2	0	4	0	0	0.04460	2.8450
c	$Cu(Al) + Cu(Al) + Ti(Al) + Cu(Al) + Ti(Al)_2 + Cu(Al)$	2	0	4	0	0	0.04578	2.8451
d	$Cu(Al) + Ti(Al)_2 + Cu(Al)_2 + Ti(Al) + Cu(Al) + Cu(Al)$	2	0	4	0	0	0.04588	2.8451
e	$Cu(Al) + Cu(Al)_2 + Ti(Al)_2 + Cu(Al)_2 + Ti(Al)_{2,f,2} + Cu(Al)_{f,2}$	2	0	4	0	0	0.04796	2.8454
f	$Cu(Al) + Ti(Al)_2 + Cu(Al)_2 + Cu(Al)_2 + Cu(Al)_2 + Ti(Ni)_{1,1,1,1,1} + Ni(Al)_{1,f,2}$	1	1	4	0	1	0.12831	2.8517
g	$Cu(Al) + Ti(Al)_2 + Cu(Al)_2 + Cu(Al)_2 + Ni(Al)_{2,f,2} + Ti(Ni)_{f,1,1} + Cu(Al)_{1,f,2}$	1	1	4	0	1	0.15883	2.8546
h	$Ti(Ni) + Ti(Ni)_2 + Cu(Al)_{1,1} + Cu(Al)_{2,1,1} + Ni(Al)_{f,2,1,1} + Cu(Al)_{2,f,f,1} + Cu(Al)_{2,\ldots,1} + Ni(Al)_{2,f,2,2,f,1,1}$	0	2	4	0	2	0.18520	2.8565
i	$Cu(Ni) + Ni(Al)_1 + Ti(Ni)_1 + Ni(Al)_1 + Cu(Ni)_{1,f,f,2} + Ni(Al)_{1,\ldots,1} + Ti(Al)_{2,1} + Cu(Ni)_1 + Ni(Al)_1 + Cu(Ni)_{\ldots,1,f,1} + Ni(Al)_1$	1	1	0	4	5	0.22614	2.8609
j	$Cu(Ni) + Cu(Al)_1 + Ti(Ni)_1 + Cu(Ni)_{\ldots 2} + Ni(Al)_1 + Ni(Al)_{f,1,1} + Cu(Al)_{2,2,1} + Ti(Ni)_1 + Ni(Al)_{1,\ldots,1} + Ni(Al)$	0	2	2	2	4	0.27844	2.8651
k	$Cu(Ni) + Ni(Al)_1 + Ni(Al)_{2,1} + Ni(Al)_{2,f,1} + Ti(Ni)_{1,1} + Cu(Ni)_{f,1} + Cu(Ni)_{\ldots 2} + Ni(Al)_1 + Ni(Al)_{2,1} + Ti(Ni)_1 + Cu(Ni) + Ni(Al)_1$	0	2	0	4	6	0.28864	2.8661
l	$Ti(Ni) + Cu(Al)_1 + Cu(Al)_2 + Cu(Al)_2 + Ni(Al)_{2,f,2,1} + Cu(Al)_2 + Ni(Al)_{2,f,2} + Ti(Ni)_1$	0	2	4	0	2	0.31041	2.8682
m	$Cu(Ni) + Ni(Al)_1 + Cu(Ni)_1 + Ni(Al)_{1,f,1} + Ti(Ni)_1 + Ni(Al)_1 + Cu(Ni)_1 + Ni(Al)_1\ Ni(Al)_{f,1,\ldots,1} + Ti(Ni) + Cu(Ni)_2 + Ni(Al)_{1,1,f,f,1} +$	0	2	0	4	6	0.32964	2.8701

first choice of Ti for Al sites, overriding Cu's preference for Al sites; (3) creation of antistructure Al atoms when the number of Ti atoms exceeds the number of available Al sites (*i.e.*, for $N_{Al} > 34$); (4) clustering of Ti(Al) around Al(Ni) antisite defects; (5) clustering of Cu(Al) around Ti(Al) (at NNN distance); and (6) decoupling between Ti(Al) and Cu atoms when Cu goes to available Ni sites.

The $N_{Cu} = 2$ ($Ni_{[38-x]}Al_{[30+x]}Ti_{[2]}Cu_{[2]}$, ($x = 1, \ldots, 5$)), shown in Figure 9, provides information on the interaction between Cu atoms and the enhanced competition between Ti and Cu additions with increasing Cu concentration. A common feature of the alloys in this set continues to be the absolute preference of Ti for Al sites and the ensuing creation of antistructure Al atoms when Al sites become unavailable. The Ti(Al) clusters form around the Ni antistructure atom. If Al sites are available, Cu(Al) atoms couple to Ti(Al) atoms, but as more Cu moves to the Ni sublattice, the coupling with Ti(Al) is replaced by either complete decoupling (as in $Ni_{[34]}Al_{[34]}Ti_{[2]}Cu_{[2]}$) or attraction with other Cu atoms (as in $Ni_{[33]}Al_{[35]}Ti_{[2]}Cu_{[2]}$). The $N_{Cu} = 3$ group ($Ni_{[38-x]}Al_{[29+x]}Ti_{[2]}Cu_{[3]}$, for $x = 1, \ldots, 5$), shown in Figure 10, highlights the behavior of Cu, as its percentage now exceeds that of Ti. The only additional feature observed in this group, a consequence of the increased Cu content, consists of the apparent clustering of Cu atoms (either in the Ni or Al sublattice), decoupled from any Ti(Al) atoms. The diagrams in Figure 10 succinctly show the competition between Ti-Cu ordering in the Al sublattice and the clustering of Cu atoms in either sublattice. The $N_{Cu} = 4$ group ($Ni_{[38-x]}Al_{[28+x]}Ti_{[2]}Cu_{[4]}$, for $x = 1, \ldots, 5$), shown in Figure 11, displays trends already apparent from the previous cases. Although no new features are observed, the larger number of Ti and Cu atoms helps to understand the main characteristic of the Ni:Al 1:1 alloys, where most additions are in solution and the clustering tendencies clearly observed in other systems are much less pronounced (*i.e.*, coupling of Ti(Al) and Cu(Al) atoms or clustering of Cu atoms in either sublattice). In all cases, as expected, the minimum energy occurs for $Ni_{[a]}Al_{[b]}Ti_{[2]}Cu_{[c]}$ alloys, where $b + c + 2 = a$, and where no antistructure atoms exist. In terms of changes in the lattice parameter, it is observed that in all cases the increase in Al concentration is the only source of such changes, due to the small difference in size between Ni and Cu atoms.

It is interesting to group the results, individually shown in Figures 7 through 11, in one single figure as a function of Ni, Al, and Cu concentration, as shown in Figure 12. Visual examination provides an indication of the characteristic features of each region in the range of concentrations studied: the Ti-Cu ordering in the Al sublattice that characterizes alloys where $N_{Ni} > N_{Al}$ transitions to an intermediate regime where no specific pattern dominates ($N_{Ni} \sim N_{Al}$), to be replaced later by another ordering pattern in the Ni sublattice (for Al-rich alloys) governed by Cu-Cu interactions.

IV. DISCUSSION: LOCAL ENVIRONMENT APPROACH

The picture that emerges from Figure 12, while retaining the essential features already observed in Monte Carlo simulations, describes the results of the interaction between different alloying additions, Ti and Cu, as a function of composition. To gain a proper understanding of this interaction, it is useful to perform an atom-by-atom energy analysis

a. $Ni_{[37]}Al_{[33]}Ti_{[2]}$
-0.57937 / 2.8536
$Ni(Al)+Ti(Al)_2+Ti(Al)_{3,2}$
Excess Ni(Al), two direct Ti(Al) substitutions

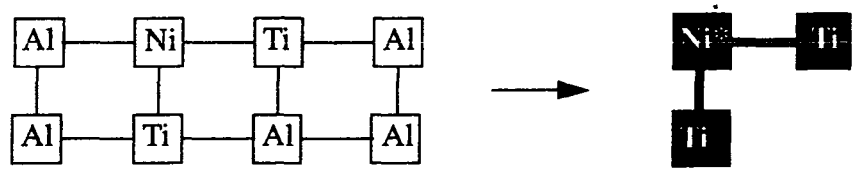

b. $Ni_{[36]}Al_{[34]}Ti_{[2]}$
-0.58580 / 2.8580
$Ti(Al)+Ti(Al)_f$
Two direct Ti(Al) in solution

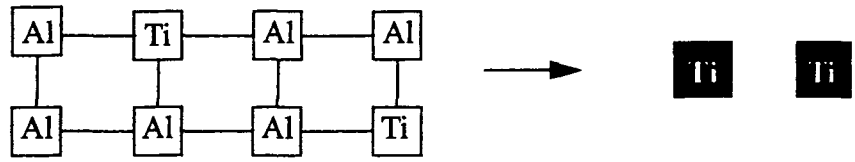

c. $Ni_{[35]}Al_{[35]}Ti_{[2]}$
-0.52298 / 2.8690
$Ti(Al)+Ti(Al)Al(Ni)_{1,1}$
One direct, one 'forced' Ti(Al), linked by Al(Ni)

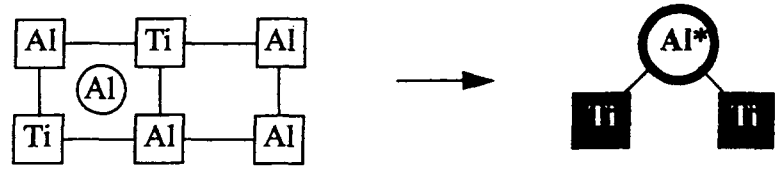

d. $Ni_{[34]}Al_{[36]}Ti_{[2]}$
-0.46710 / 2.8793
$Ti(Al)Al(Ni)_1+Ti(Al)Al(Ni)_{1,2}$
Two 'forced' Ti(Al) substitutions, linked by both Al(Ni) atoms

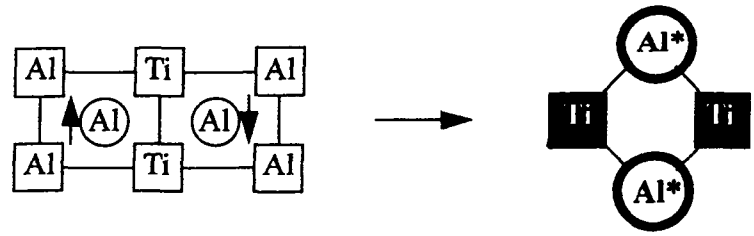

e. $Ni_{[33]}Al_{[37]}Ti_{[2]}$
-0.41384 / 2.8900
$Al(Ni)+Ti(Al)Al(Ni)_{1,2}$
$+Ti(Al)_1Al(Ni)_{1,2,2}$
Excess Al(Ni), two forced Ti(Al) atoms linked by Al(Ni) atoms.

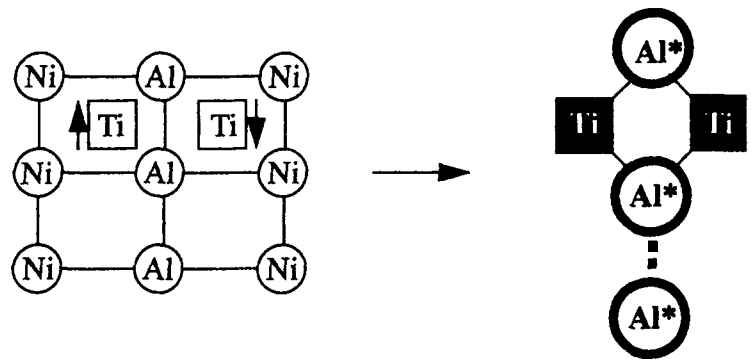

Fig. 7—(*a*) through (*e*) Ground state configurations including the energy of formation (in eV/atom), lattice parameter (in Angstroms) and structural information for $Ni_{[38-x]}Al_{[32+x]}Ti_{[2]}$, for $x = 1, \ldots, 5$. Squares denote atoms in the Al sublattice, while circles denote atoms in the Ni sublattice. The arrows in (d) and (e) indicate whether the atom is in a plane above (up) or below (down) the plane of the page. On the right, a simpler, schematic diagram summarizes the principal features of the atomic distributions shown on the left, concentrating only on the defect structure. Solid vertical or horizontal lines indicate bonds in an Al plane, while solid diagonal lines (c, d, e) indicate bonds between an atom in the Al sublattice and its NN in the Ni sublattice. Dashed vertical or horizontal lines indicate NNN bonds between atoms in the Ni sublattice. Al* denotes an antistructure Al atom, Al(Ni), and Ni* denotes an antistructure Ni atom, Ni(Al).

in order to identify the trends and reasons for the observed behavior. A simple approach, based on the BFS energy contributions for a given defect and its surroundings, helps explain the observed behavior in Ni-Al-Ti-Cu alloys, as well as the magnitude of the energy gaps that characterize the various defect structures observed in the energy spectra of the alloys studied. Based on the energetics of small groups of atoms surrounding specific atoms in the cell, the idea consists of analyzing the resulting site substitution behavior not just in terms of individual interactions between individual atoms, but through the effect that these bonds might have in the immediate vicinity of such atoms.

In order to implement this approach, we define atomic "local environments" (LEs)[18] consisting of a given central

a. $Ni_{[37]}Al_{[32]}Ti_{[2]}Cu_{[1]}$
-0.57330 / 2.8502
$Ni(Al)+Ti(Al)_2+Cu(Al)_2+Ti(Al)_{2,f,2}$
Excess Ni(Al), two direct Ti(Al) and one direct Cu(Al) substitutions.

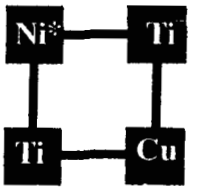

b. $Ni_{[36]}Al_{[33]}Ti_{[2]}Cu_{[1]}$
-0.58227 / 2.8545
$Ti(Al)+Cu(Al)_2+Ti(Al)_2$
Two direct Ti(Al) and one Cu(Al) substitutions, linking both Ti(Al) atoms.

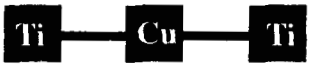

c. $Ni_{[35]}Al_{[34]}Ti_{[2]}Cu_{[1]}$
-0.57239 / 2.8608
$Ti(Al)+Ti(Al)_f+Cu(Ni)_{f,f}$
Two direct Ti(Al), one direct Cu(Ni) substitution in solution.

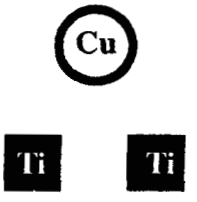

d. $Ni_{[34]}Al_{[35]}Ti_{[2]}Cu_{[1]}$
-0.51152 / 2.8714
$Ti(Al)+Ti(Al)Al(Ni)_1+Cu(Ni)_2$
One direct, one 'forced' Ti(Al) substitutions, linked by both Al(Ni) atoms, and one direct Cu(Ni) substitution linked to Al(Ni), but not to Ti(Al).

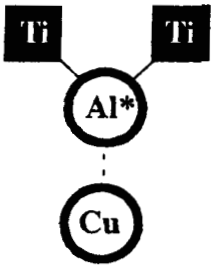

e. $Ni_{[33]}Al_{[36]}Ti_{[2]}Cu_{[1]}$
-0.45967 / 2.8834
$Ti(Al)Al(Ni)_1+Ti(Al)Al(Ni)_{1,2}+Cu(Ni)_2$
Two forced Ti(Al) atoms linked by Al(Ni) atoms. One direct Cu(Ni) linked to Al(Ni) but not to Ti(Al).

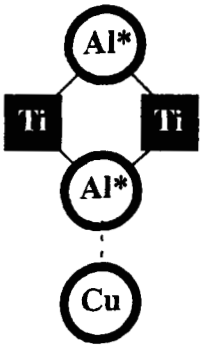

Fig. 8—(*a*) through (*e*) Ground state configurations for $Ni_{[38-x]}Al_{[31+x]}Ti_{[2]}Cu_{[1]}$, for $x = 1, \ldots, 5$.

atom and its eight NN and six NNN (in a bcc lattice), under the assumption that it is this group of atoms that will be most affected by the presence of a central substitutional defect atom and that any change in the energy of formation of the cell will arise mostly from changes in energy within this environment. Considering the fact that the BFS equations deal with up to second neighbors of a given atom, and that no individual relaxations are allowed, it is then sufficient to examine the energetics of this limited group of atoms in order to understand the full effect of a given point defect

a. $Ni_{[37]}Al_{[31]}Ti_{[2]}Cu_{[2]}$
-0.56688 / 2.8468
$Ni(Al)+Ti(Al)_2+Ti(Al)_{f,2}+Cu(Al)_2+Cu(Al)$
Excess Ni(Al), two direct Ti(Al) and two direct direct Cu(Al) substitutions.

b. $Ni_{[36]}Al_{[32]}Ti_{[2]}Cu_{[2]}$
-0.57529 / 2.8512
$Ti(Al)+Cu(Al)_2+Ti(Al)_2+Cu(Al)_{2,f,2}$
Two direct Ti(Al) and Cu(Al) substitutions.

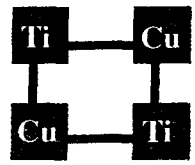

c. $Ni_{[35]}Al_{[33]}Ti_{[2]}Cu_{[2]}$
-0.56617 / 2.8574
$Cu(Ni)+Cu(Al)_1+Ti(Al)_2+Ti(Al)$
Two direct Ti(Al), one direct Cu(Ni) linked to Cu(Al).

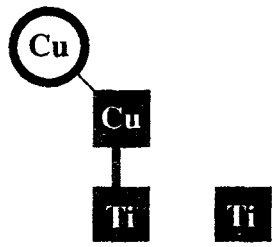

d. $Ni_{[34]}Al_{[34]}Ti_{[2]}Cu_{[2]}$
-0.55662 / 2.8636
Ti(Al)+Ti(Al)+Cu(Ni) + Cu(Ni)
Two direct Ti(Al) substitutions and two direct Cu(Ni) substitutions, in solution.

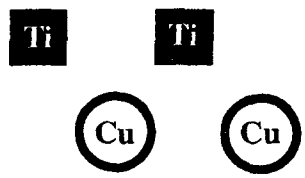

e. $Ni_{[33]}Al_{[35]}Ti_{[2]}Cu_{[2]}$
-0.49871 / 2.8740
$Ti(Al)Al(Ni)_1+Ti(Al)_1+Cu(Ni)+Cu(Ni)_2$
One direct and one forced Ti(Al) atom linked by Al(Ni). One direct Cu(Ni) linked to Al(Ni) but not to Ti(Al).

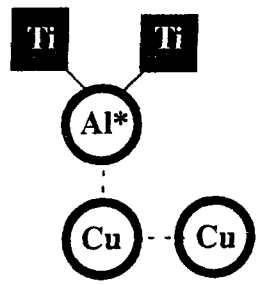

Fig. 9—(*a*) through (*e*) Ground state configurations for $Ni_{[38-x]}Al_{[30-x]}Ti_{[2]}Cu_{[2]}$, for $x = 1, \ldots, 5$.

(*i.e.*, substitution of one atom by another, creation of a single vacancy, *etc.*). As an example, the LE of an individual X(B) defect, denoted by $\langle X(B)\rangle$, is shown in Figure 13. The $\langle X(B)\rangle$ consists of an X atom in a site in the B sublattice of an A-B alloy, surrounded by eight NN of type A and six NNN of type B. The formation of an antisite defect, X(A)A(B), could then be seen as the superposition of the LE surrounding two individual point defects: one centered around the X atom, $\langle X(A)\rangle$, and the other centered around the displaced A atom, $\langle A(B)\rangle$. These could be "noninteracting." $\langle [X(A)A(B)]_f\rangle$ (if the two point defects are separated by more than one lattice parameter distance), or "overlapping." $\langle [X(A)A(B)]_1\rangle$, LEs,

a. $Ni_{[37]}Al_{[30]}Ti_{[2]}Cu_{[3]}$
-0.55866 / 2.8437
$Ni(Al)+Ti(Al)_2+Cu(Al)_2+Ti(Al)_2+Cu(Al)_{2,f,2}+Cu(Al)_{f,2}$
Excess Ni(Al), two Ti(Al) and three direct Cu(Al) substitutions

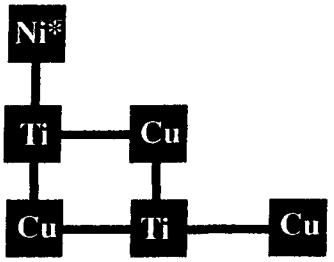

b. $Ni_{[36]}Al_{[31]}Ti_{[2]}Cu_{[3]}$
-0.56789 / 2.8480
$Ti(Al)+Cu(Al)_2+Ti(Al)_2+Cu(Al)_{2,f,2}+Cu(Al)_{...2}$
Two direct Ti(Al) and three direct Cu(Al) substitutions

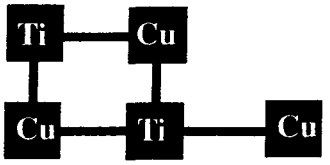

c. $Ni_{[35]}Al_{[32]}Ti_{[2]}Cu_{[3]}$
-0.55847 / 2.8541
$Ti(Al)+Cu(Al)_2+Cu(Al)+Cu(Ni)_1+Ti(Al)$
Two direct Ti(Al), one direct Cu(Ni) linked to Cu(Al)

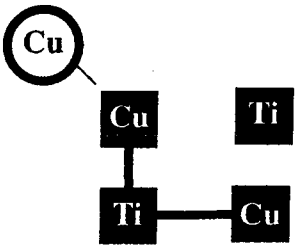

d. $Ni_{[34]}Al_{[33]}Ti_{[2]}Cu_{[3]}$
-0.55085 / 2.8602
$Ti(Al)+Ti(Al)+Cu(Ni)+Cu(Al)_1+Cu(Ni)_1$
Two direct Ti(Al) substitutions, one Cu(Al) and two Cu(Ni) substitutions, with clustering of Cu atoms.

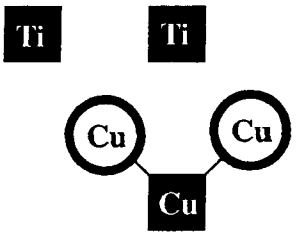

e. $Ni_{[33]}Al_{[34]}Ti_{[2]}Cu_{[3]}$
-0.54248/ 2.8663
$Ti(Al)_1+Ti(Al)+Cu(Ni)+Cu(Ni)_2+Cu(Ni)_2$
Two direct Ti(Al) atoms in solution, a cluster of three direct Cu(Ni) atoms, not coupled to any Ti(Al) atom

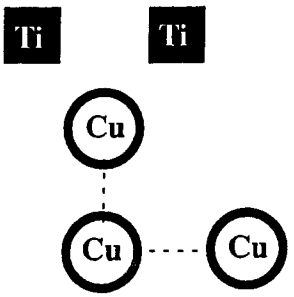

Fig. 10—(*a*) through (*e*) Ground state configurations for $Ni_{[38-x]}Al_{[29+x]}Ti_{[2]}Cu_{[3]}$, for $x = 1, \ldots, 5$.

where the two center atoms (X and A) are NN, thus sharing a large number of NN and NNN atoms. The latter case is shown in Figure 13(b).

To make a fair comparison of the different single and extended local environments, it is necessary to embed each LE in a B2 cell so that all bonds affected by the presence

a. $Ni_{[37]}Al_{[29]}Ti_{[2]}Cu_{[4]}$
-0.55125 / 2.8406
$Ni(Al)+Ti(Al)+Cu(Al)_2+Ti(Al)_2+Cu(Al)_2+Cu(Al)_{f,2}$
Excess Ni(Al), two Ti(Al) and four direct Cu(Al) substitutions.

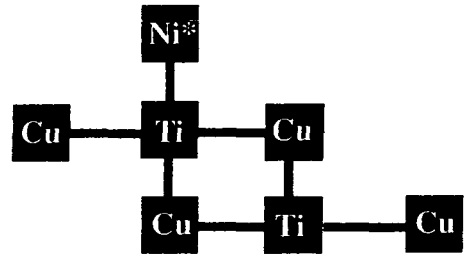

b. $Ni_{[36]}Al_{[30]}Ti_{[2]}Cu_{[4]}$
-0.56030 / 2.8450
$Ti(Al)+Cu(Al)_2+Ti(Al)_2+Cu(Al)_{2,f,2}+Cu(Al)_{-2}$
Two direct Ti(Al) and four direct Cu(Al) substitutions.

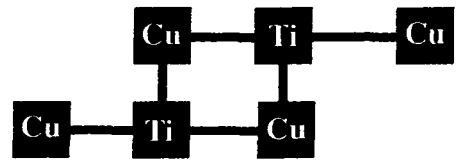

c. $Ni_{[35]}Al_{[31]}Ti_{[2]}Cu_{[4]}$
-0.55338 / 2.8507
$Ti(Al)+Cu(Al)_2+Ti(Al)+Cu(Al)_{2,f,2}+Cu(Ni)_1+Cu(Al)_1$
Two direct Ti(Al), one direct Cu(Ni) linked to Cu(Al).

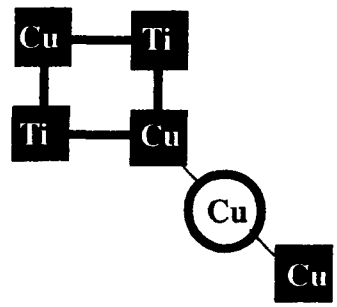

d. $Ni_{[34]}Al_{[32]}Ti_{[2]}Cu_{[4]}$
-0.54786 / 2.8564
$Ti(Al)+Cu(Al)_2+Ti(Al)_2+Cu(Al)_{2,2}+Cu(Ni)_1+Cu(Ni)_2$
Two direct Ti(Al) substitutions, two Cu(Al) and two Cu(Ni) substitutions, with clustering of Cu atoms.

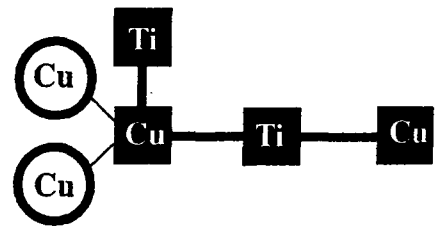

e. $Ni_{[33]}Al_{[33]}Ti_{[2]}Cu_{[4]}$
-0.53742 / 2.8628
$Ti(Al)+Cu(Al)2+Cu(Ni)1+Cu(Ni)_{2,1}+Ti(Al)+Cu(Ni)$
Two direct Ti(Al) atoms in solution, one Cu(Al) and three direct Cu(Ni) atoms, not coupled to any Ti(Al) atom.

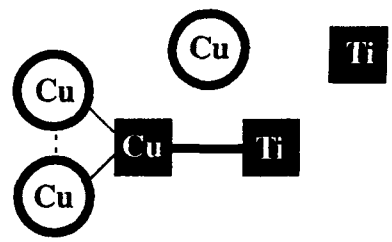

Fig. 11—(*a*) through (*e*) Ground state configurations for $Ni_{[38-x]}Al_{[28+x]}Ti_{[2]}Cu_{[3]}$, for $x = 1, \ldots, 5$.

of the defect are accounted for. To do so, we locate the LE at the center of a 72-atom equilibrium B2 NiAl cell and refer all energies to the pure AB version of that cell. Because all LEs, as well as the reference B2 cell, are evaluated at the same lattice parameter, the energy difference between the cell with the defect and the reference cell, Δe, indicates

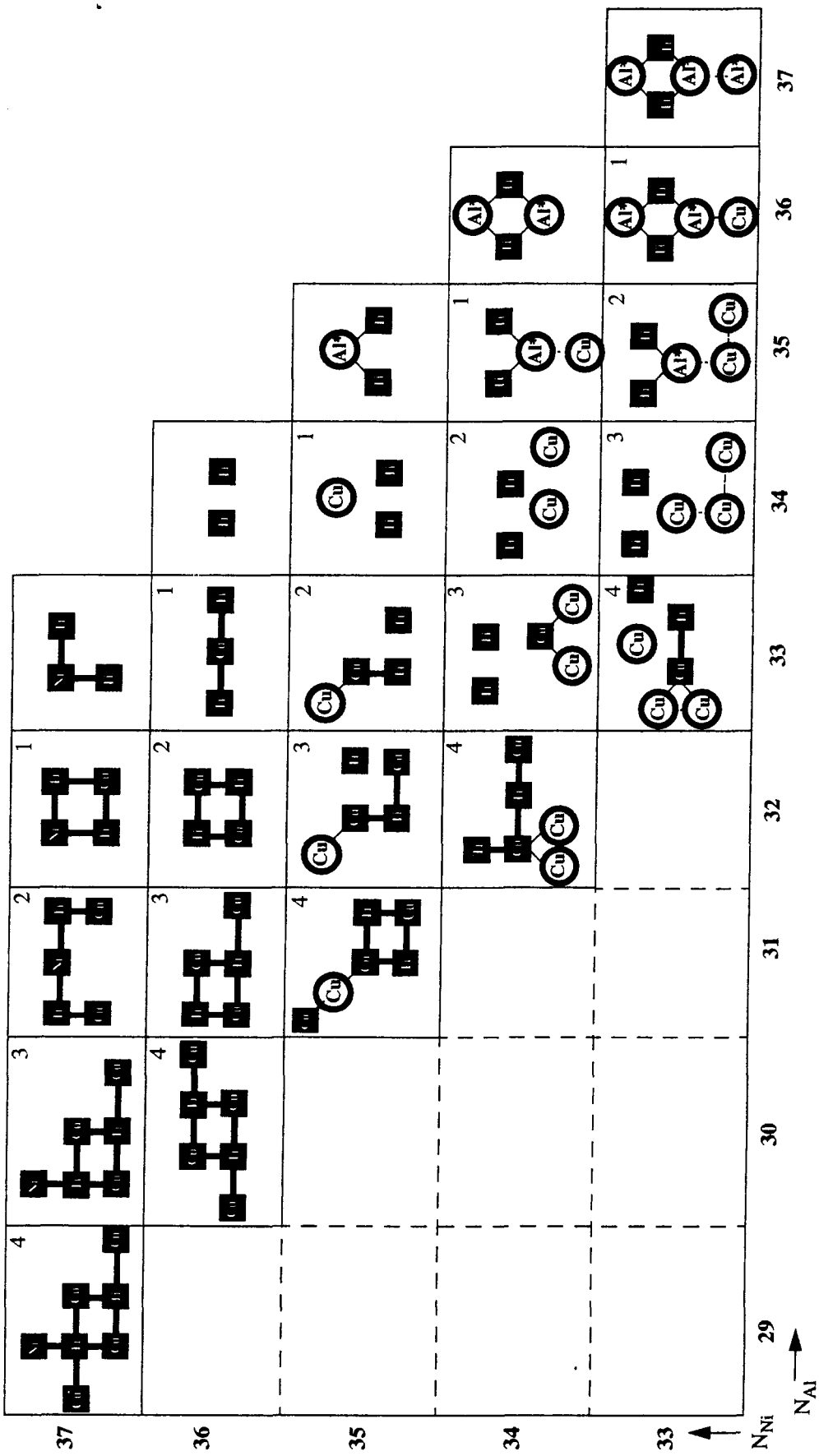

Fig. 12—Summary of Figs. 7 through 11, showing the basic scheme that describes the ground state for each alloy modeled (Fig. 1). Fig. 7 provides notation. Squares (circles) denote atoms in the Al (Ni) sublattice. Connected squares (circles) indicate NN bonds and isolated squares (circles) denote atoms that are separated by distances greater than NN distance. The ground state structures range from patterned Ti(Al) and Cu(Al) substitutions (upper left corner) to Ti(Al) and Cu(Ni) substitutions (lower right). Ni and Al content is indicated along the vertical and horizontal axes, respectively. Every configuration includes two Ti atoms and Cu is balance, as indicated by the number in the upper right corner of each box.

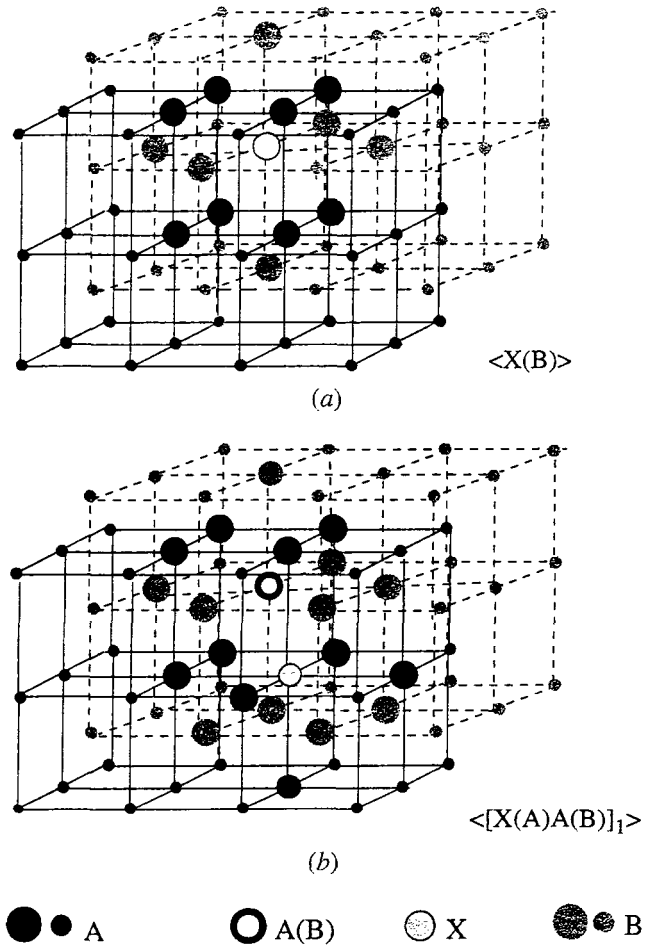

Fig. 13—(*a*) ⟨X(B)⟩ local environment: X atom (light gray) in a B site, surrounded by eight A NN (large black disks) and six B NNN (large gray disks). (*b*) ⟨[X(A)A(B)]$_1$⟩, with the substitutional X atom in an A site and the displaced A atom (circle) in a B site. The two "defect" atoms (the substitutional X and antistructure A) are NN and are surrounded by an environment of 20 atoms, accounting for all the NN and NNN, some of which are shared between them. A or B atoms at distances greater than one lattice parameter from either one of the defect atoms are indicated with small black and gray disks, respectively.

the energy cost (in terms of chemical energy differences) of performing the specific substitutions that characterize the defect (as it contains only the contributions from the atoms in the LE, and not the rest of the cell).

Table IV lists the energy of formation (relative to an ideal B2 NiAl cell) of different local environments: ⟨X(B)⟩ and ⟨X(A)⟩ (for X = Ti or Cu and A and B = Ni or Al), ⟨Ni(Al)⟩ and ⟨Al(Ni)⟩. The corresponding values for the extended local environments, including two substitutions, are also listed. It is reasonable to expect that the site preference is mainly determined by the relative energy of formation $\Delta e\{\text{LE}\}$ of these local environments. For example, if $\Delta e\{\langle \text{X(B)}\rangle\} < \Delta e\{\langle [\text{X(A)A(B)}]_f\rangle\}$ or $\Delta e\{\langle \text{X(B)}\rangle\} < \Delta e\{\langle [\text{X(A)A(B)}]_1\rangle\}$, then X chooses a site in the B sublattice, as the formation of a single ⟨X(B)⟩ entails a lower energy cost than that required by the combination of a substitutional defect and the creation of an antistructure A atom, regardless of the relative position of these defects. For consistency, this analysis has to be performed in unrelaxed atomic positions,

Table IV. BFS Energy of Formation of Single and Double Local Environments (in eV/Atom), Relative to a 72-atom B2 Cell; for the Double-Centered LE, the Center Atoms Are Located at NN ($[]_1$), NNN ($[]_2$), or Greater Than NNN Distance ($[]_f$); the Subindex *H* ($[]_H$) Indicates That the Center Atoms (Ti and Cu) Locate Themselves Following a Heusler ($L2_1$) Pattern in the Al Sublattice (*i.e.*, Sharing an Al Atom as a NNN)

LE	Δe_T	LE	Δe_T
⟨Ni(Ni)⟩	0.00000	⟨[Cu(Al) + Ni(Al)]$_f$⟩	0.01988
⟨Ni(Al)⟩	0.01099	⟨[Cu(Al) + Ni(Al)]$_2$⟩	0.02151
⟨Al(Ni)⟩	0.09434	⟨[Al(Ni) + Cu(Al)]$_f$⟩	0.10323
⟨Ti(Al)⟩	0.00772	⟨[Al(Ni) + Cu(Al)]$_1$⟩	0.09369
⟨Ti(Ni)⟩	0.16333	⟨[Ti(Al) + Ti(Al)]$_f$⟩	0.01544
⟨Cu(Ni)⟩	0.01651	⟨[Ti(Al) + Ti(Al)]$_2$⟩	0.01647
⟨Cu(Al)⟩	0.00889	⟨[Ti(Al) + Ti(Al)]$_H$⟩	0.01593
⟨[Ti(Al) + Al(Ni)]$_f$⟩	0.10205	⟨[Cu(Al) + Cu(Al)]$_f$⟩	0.01778
⟨[Ti(Al) + Al(Ni)]$_1$⟩	0.08739	⟨[Cu(Al) + Cu(Ni)]$_f$⟩	0.02540
⟨[Ti(Al) + Cu(Al)]$_2$⟩	0.01497	⟨[Cu(Al) + Cu(Ni)]$_1$⟩	0.02377
⟨[Ti(Al) + Cu(Al)]$_H$⟩	0.01622	⟨[Ti(Ni) + Ni(Al)]$_1$⟩	0.15060
⟨[Ti(Al) + Cu(Al)]$_f$⟩	0.01661	⟨[Ti(Ni) + Ni(Al)]$_f$⟩	0.17431
⟨[Ni(Al) + Ti(Al)]$_f$⟩	0.01870	⟨[Ni(Al) + Cu(Ni)]$_1$⟩	0.02598
⟨[Ni(Al) + Ti(Al)]$_2$⟩	0.01703	⟨[Ni(Al) + Cu(Ni)]$_f$⟩	0.02750

under the assumption that relaxation effects, while influential, are not ultimately responsible for the observed site preference behavior.

A. *Local Environment Analysis of Atomic Coupling*

In this approach, it is as important to isolate individual patterns and establish a hierarchy of effects by means of their relevance as measured by the typical energies involved, as it is to first gain understanding of the behavior of individual additions before examining the effect of their interactions. We start with the LE study of ternary additions (Ti or Cu) to NiAl, followed by the quaternary case (Ti and Cu interactions in NiAl). In the ternary cases, where the goal is to identify the reasons that explain the different site substitution options, it is not necessary to consider the relative locations of the substitutional and antistructure atoms. While impor-tant, the gain or loss of energy due to different relative positions is not comparable in magnitude with the corresponding gain or losses due to substitutions themselves.

1. *Ti site preference in NiAl*

The relevant results listed in Table IV are shown in Figures 14(a) and (b), which schematically represent the energy cost (in terms of the energy of formation of unrelaxed LEs) in creating substitutional defects and antistructure atoms for Ni-rich (Figure 14(a)) and Al-rich alloys (Figure 14(b)).

For Ni-rich alloys, which contain available Al sites, the competition between Ti(Al) and Ti(Ni)Ni(Al) substitutions is explained by the high energy cost of the Ti(Ni) substitution (⟨Ti(Ni)⟩), which, compounded with the small energy cost of creating a Ni antistructure atom (⟨Ni(Al)⟩), results in an almost insurmountable energy gap greatly favoring Ti(Al) substitutions: $\Delta e\{\langle \text{Ti(Ni)Ni(Al)}\rangle_f\} - \Delta e\{\langle \text{Ti(Al)}\rangle\} = 0.16660$ eV/atom. In Al-rich alloys (Ni available sites), it is the high energy cost of creating an antistructure Al atom that dominates the site preference

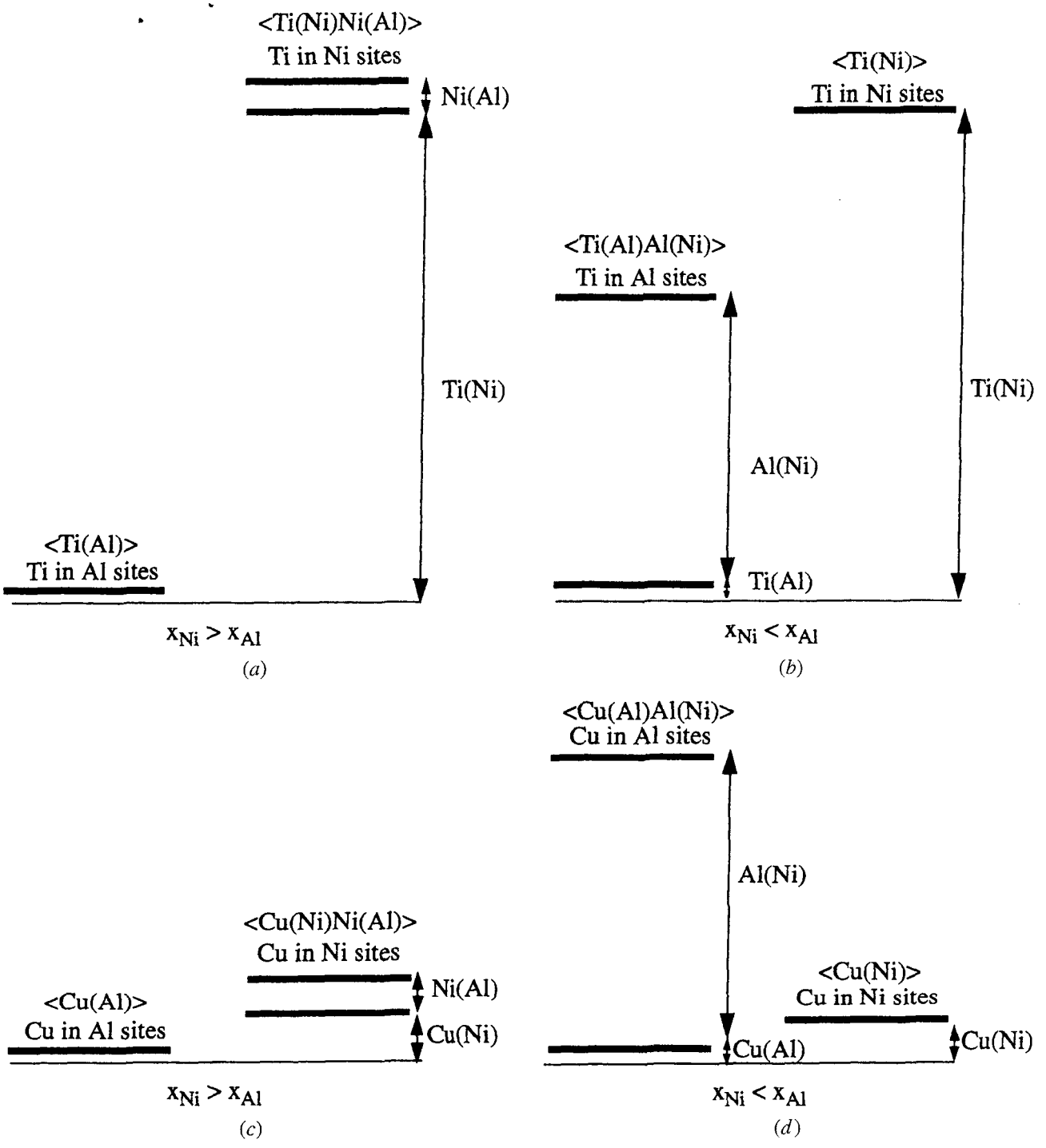

Fig. 14—Energy level diagram for the energies of formation of different local environments needed to describe the site preference behavior of (*a*) Ti in Ni-rich, (*b*) Ti in Al-rich, (*c*) Cu in Ni-rich, and (*d*) Cu in Al-rich NiAl alloys. The left diagrams indicate the possible substitutions in Ni-rich alloys, indicating a clear preference for Al sites for Ti and Cu. The diagrams on the right correspond to Al-rich alloys, still showing a clear (but less marked) Ti preference for Al sites and Cu preference for Ni sites. The energies are referenced to a pure B2 NiAl alloy.

behavior, as seen in Figure 14(b). However, in spite of being large ($\Delta e\{\langle \text{Al(Ni)} \rangle\} = 0.09434$ eV/atom), the combination of a Ti(Al) and a Al(Ni) substitution still does not match the high energy cost of locating a Ti atom in a Ni site. The energy gap between Ti(Ni) and Ti(Al)Al(Ni) defects in Al-rich alloys, $\Delta e\{\langle \text{Ti(Ni)} \rangle\} - \Delta e\{\langle \text{Ti(Al)Al(Ni)} \rangle_f\} = 0.06127$ eV/atom, is not as large as the one between Ti(Ni)Ni(Al) and Ti(Al) defects in Ni-rich alloys, indicating that, while the preference of Ti for Al sites is shared by Ni-rich and Al-rich alloys, it is weaker for the latter, consistent with the results of the Monte Carlo simulations where there was an increasing proportion of Ti atoms finding their way to the Ni sublattice for Al-rich alloys.

2. *Cu site preference in NiAl*

The analysis of Cu additions to NiAl is shown in Figures 14(c) and (d). For Ni-rich alloys (Figure 14(c)), the energy

cost of locating a Cu atom in a Ni site, added to a comparable energy cost for creating a Ni antisite defect, results in a net preference for Al sites, although not of the same magnitude as that found for Ti in a similar situation. The proximity between the energy levels corresponding to Cu(Al) and Cu(Ni)Ni(Al)$_f$ can be understood as more options become available for Cu, which can be easily excited to reside in a Ni site with low energy cost. For Al-rich alloys, in spite of the fact of the direct preference of Cu for Al sites ($\Delta e\{\langle \text{Cu(Al)} \rangle\} = 0.00889$ eV/atom *vs* $\Delta e\{\langle \text{Cu(Ni)} \rangle\} = 0.01651$ eV/atom), the high energy cost of creating an antisite Al defect erases the advantage of direct Cu substitutions for Al sites, making Ni sites a favorable choice.

B. *Ti and Cu Additions and Interaction between Point Defects*

Before continuing with a detailed analysis of the quaternary case, some conclusions can be extracted from the ternary cases, as described in Figure 14. It is interesting to compare the Cu energy level diagrams with those obtained for Ti in spite of the fact that both elements display a "direct" preference for Al sites regardless of composition (*i.e.*, either Ti or Cu is energetically more stable in an Al site than in a Ni site). Comparing Figures 14(a) and (b) with Figures 14(c) and (d) and the corresponding LE formation energies in Table IV, the energy difference between Cu(Al) and Cu(Ni)Ni(Al) substitutions is only 0.01861 eV/atom, an order of magnitude smaller than that found for Ti. This fact, coupled with the smaller energy cost in locating Ti atoms in Al sites in Ni-rich alloys than the much larger one required for substitutions in Ni sites, justifies the observed prevalence of Ti in using the available sites in the Al sublattice. Conversely, for Al-rich alloys, the resulting energy difference between Cu(Al)Al(Ni) and Cu(Ni) substitutions (0.08672 eV/atom) explains the ease with which Cu favors sites in the Ni sublattice instead of competing with Ti for Al sites. It could then be assumed that if this behavior continues in the case of quaternary systems, then Ti will always choose Al sites while Cu will move from Al sites to Ni sites depending on the Ni:Al ratio. This assumption, based solely on extrapolating features characterizing the ternary systems, ignores effects that could arise from the interaction between the two alloying additions. The atomic distributions shown in Figure 12 clearly indicate that the ternary site substitution behavior alone does not completely explain all the salient characteristics of each ground state, as several other features, besides the specified site preference for Ti and Cu, can be identified (Figure 12).

It is necessary to concentrate on the quaternary system and the influence of the interaction between the different elements in the resulting structures. These results indicate that the characteristic energies of the single element site preference behavior (Ti or Cu in NiAl) are of the order of 0.1 eV/atom. There are clearly secondary effects, at a lower energy scale, that also intervene in determining the final atomic distribution. Such effects arise from the coupling between the different alloying additions and should not be ignored if a proper description of the ground state is desired. Several of these effects have already been identified, although not explained, by inspecting the structure of the ground states shown in Figures 7 through 11. In what follows, we describe and quantify the nature of these effects, based on the analysis of noninteracting and overlapping LEs.

1. *Ti and Cu interaction with antisite defects*

One common feature of all the ground states shown in Fig. 12 consists of the preference of Ti for Al sites. It is interesting to discuss how Ti(Al) atoms interact with antistructure atoms, when present, or Cu alloying additions.

The top row in Figure 12 contains alloys for which it has been established that Ti and Cu additions occupy sites in the Al sublattice. Moreover, for $x_{Ni} > 50$ at. pct, there are also Ni antistructure atoms present. With these three types of atoms in the Al sublattice, we now investigate the possible coupling schemes that might appear in such systems. By coupling, we mean the interaction between different types of atoms that results in the formation of NN or, when appropriate, NNN bonds.

Among the three possible couplings, [Ti(Al) + Ni(Al)], [Cu(Al) + Ti(Al)], and [Cu(Al) + Ni(Al)], only the first two involve a gain in energy when a NNN bond is formed (*i.e.*, $\Delta e\{[]_2\} < \Delta e\{[]_f\}$). The creation of a [Ti(Ni) + Ni(Al)]$_2$ bond introduces a gain of 0.00167 eV/atom over [Ti(Al) + Ni(Al)]$_f$. This explains the observed Ti(Al) ↔ Ni(Al) coupling that characterizes the ground states of the Ni-rich quaternary alloys in the top row in Figure 12. A comparable gain is realized if a [Cu(Al) + Ti(Al)]$_2$ bond is formed. No such gain exists for [Cu(Al) + Ni(Al)]$_2$ bonds, thus establishing a coupling scheme Cu(Al) ↔ Ti(Al) ↔ Ni(Al). Table IV also shows that the local environment energy of Ti(Al) + Cu(Al) atoms varies little depending on the relative location of the two substitutional atoms (0.01497 eV/atom when they are located at NNN distance, 0.01661 eV/atom when they are separated by greater distances, and 0.01622 eV/atom when they are located at the opposite corners of a cube in the Al sublattice). The proximity of these three energy levels explains the ordering pattern observed, for example, in the ground state for the $Ni_{[37]}Al_{[29]}Ti_{[2]}Cu_{[4]}$ alloy.

The coupling scheme (Cu(Al) ↔ Ti(Al) ↔ Ni(Al)) results in the characteristic feature of other Ni-rich alloys, as shown in Figure 15. Some additional patterns with respect to that coupling hierarchy are also apparent. With the coupling Ti(Al) ↔ Ni(Al) firmly established, we now consider its consequences when several Ti(Al) atoms are present. Of the three cases listed in Table IV for the relative location of two substitutional Ti(Al) atoms ([Ti(Al) + Ti(Al)]$_f$, [Ti(Al) + Ti(Al)]$_2$, and [Ti(Al) + Ti(Al)]$_H$), the NNN bond is the less energetically favored, followed by the "Heusler" arrangement and, finally, with the lowest energy cost, the two atoms far apart. As mentioned previously, Ti(Al) ↔ Ni(Al) coupling will rule out this last option, thus favoring sites at third-neighbor distance (Heusler-like sites), as seen in Figure 15, where the number of favorable Ti-Al bonds is maximized. This effect can be understood as the role of Ni(Al) promoting the attraction of Ti atoms into an ordered pattern. While the link Cu(Al) ↔ Ti(Al) can be interpreted as responsible for "closing" the square formed by Ni(Al), Ti(Al), Cu(Al), and Ti(Al) (Figure 15), the "repulsion" between Cu(Al) and Ni(Al) results in a competition between the number of Ti(Al)-Ni(Al) and Cu(Al)-Ti(Al) bonds, which explains the loss of one Ti(Al)-Ni(Al) bond at the expense of extra

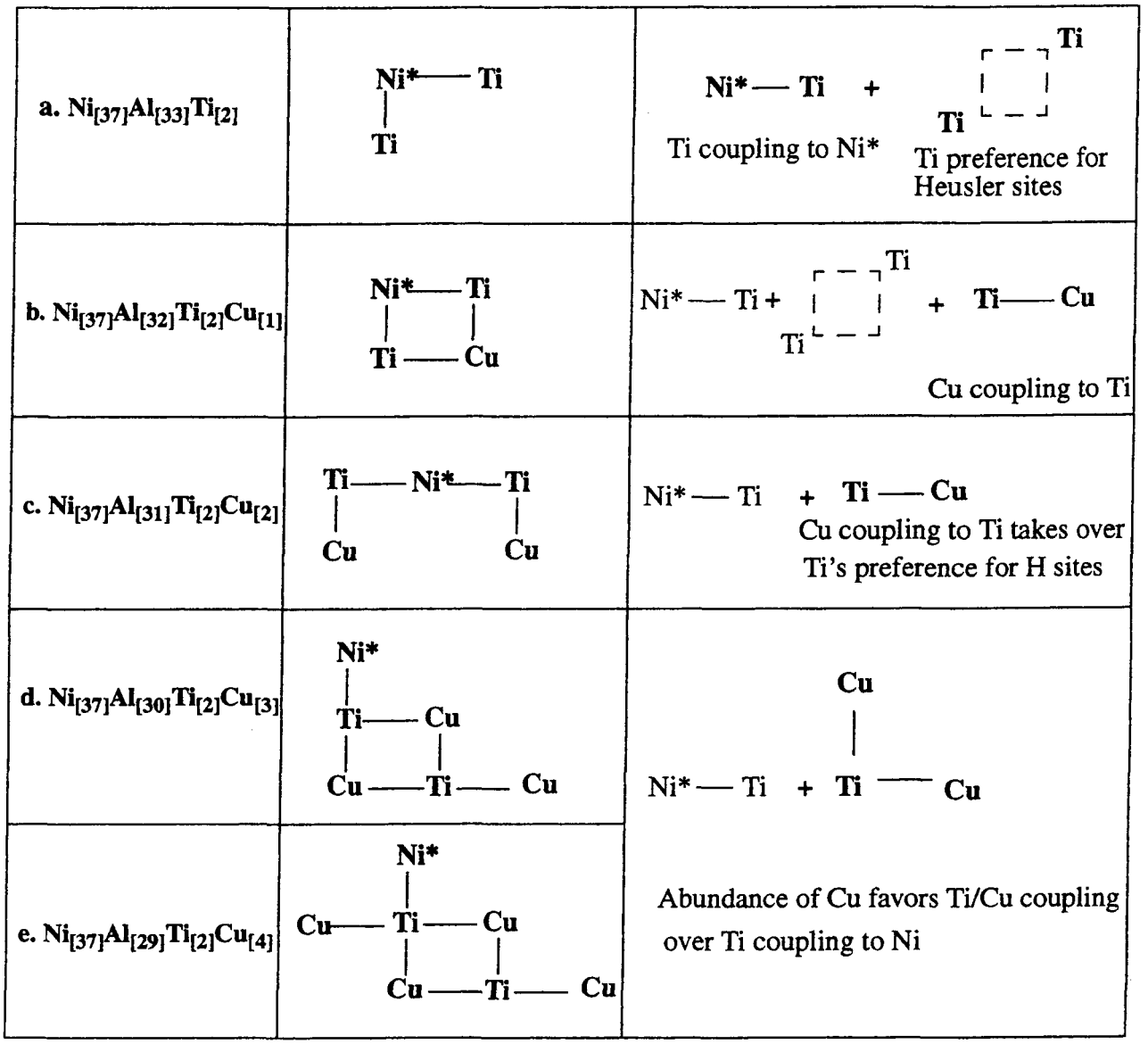

Fig. 15—Coupling series Cu ↔ Ti ↔ Ni, as manifested in Ni-rich alloys with increasing Cu content. The last column describes the individual elements, in order of importance, leading to the final state (center column).

Cu(Al)-Ti(Al) bonds, as observed in Figures 15(d) and (e). However, the alternating pattern of Cu-Ti-Cu-Ti atoms persists. This fact can be taken as a hint that in alloys with higher Ti concentration than the ones studied in this work, Cu additions might partition to the $L2_1$ (Heusler) phase.

The coupling of Ti(Al) atoms with antisite defects persists in Al-rich alloys. For these cases, the Ti(Al)-Al(Ni) coupling introduces comparable energy gains (0.01466 eV/atom) with respect to the noninteracting case. Every alloy with Al antistructure atoms shows Ti(Al)-Al(Ni) coupling, regardless of the Cu contents. Moreover, Ti(Al)-Al(Ni) coupling overrides the tendency of Ti(Al) atoms to locate themselves in Heusler sites. Overall, this coupling seems to be the leading effect relating the defects in each sublattice in these alloys: Ti(Al) substitutional atoms in the Al sublattice and Cu atoms in the Ni sublattice both bond to the available antistructure Al atoms (Figures 7(c), (e), 8(d) and (e), and 9(e)).

2. *Ti and Cu interactions*

As the number of available Al sites decreases ($N_{Ni} < 36$ in Figure 12), the leading role of Ti(Al) substitutions forces Cu atoms to occupy the remaining Al sites as well as the increasing number or Ni available sites, thus coexisting in both sublattices. Table IV indicates that the interaction between Cu(Ni) and Cu(Al) atoms involves changes in energy of similar or smaller magnitude than the ones described in Section 1. As a consequence, clustering of Cu atoms (linking Cu(Al) and Cu(Ni) atoms, as in Figures 9(c), 10(c) and (d), and 11(d) and (e)) is observed. The NN bond [Cu(Ni) + Cu(Al)]$_1$ introduces a 0.00163 eV/atom energy gain over the two atoms in solution, translating into Cu clustering in Ni-rich alloys with high Cu concentration. Finally, the smallest gains are realized by Ti(Al) atoms locating themselves at NNN distance (0.00103 eV/atom). Although small, it suffices to explain the observed trends in all alloys with

nearly the same number of Ni and Al sites where equal partitioning of Ti atoms in solution in one sublattice (Al) and Cu atoms in the other (Ni), without interaction between them, is seen.

C. *Summary of Site Occupancy Behavior*

Having discussed individual and collective behavior in the previous sections, it is useful to summarize the main features by a quick review of Figure 15. While the top row of Figure 12 highlights the role of the coupling series Cu(Al) ↔ Ti(Al) ↔ Ni(Al) in $Ni_{[37]}Al_{[34-x]}Ti_{[2]}Cu_{[x]}$ (x = 1, . . . , 5) alloys, the next lines in Figure 12 are examples of the same coupling feature but without the Ni antistructure atom, indicating that it is precisely the presence of antisite defects and other substitutional atoms (such as Cu or Hf[18]) that ties substitutional Ti atoms together. Their absence, as in alloys with N_{Al} = 33 and N_{Al} = 34, results in Ti(Al) atoms remaining in solution. The set with N_{Ni} = 35 marks the transition between the Cu(Al) ↔ Ti(Al) ↔ Ni(Al) regime, characteristic of Ni-rich alloys, to the migration of Cu atoms to the Ni sublattice that is dominant in Al-rich alloys. For example, $Ni_{[35]}Al_{[34]}Ti_{[2]}Cu_{[1]}$ represents the reduced importance of Cu-Ti coupling once Cu occupies Ni sites, while alloys with the same number of Ni atoms but increasing Cu content highlight the dual role of Cu linking Ti atoms when residing in Al sites and leading to Cu clustering when occupying sites in either sublattice. The NN bonds Cu(Ni)-Cu(Al) compete with Cu(Al)↔Ti(Al), thus explaining the small energy advantage of $Ni_{[35]}Al_{[33]}Ti_{[2]}Cu_{[2]}$ (as shown in Figure 12) over a similar distribution where the isolated Ti atom is linked to both Cu(Al) and Cu(Ni), or, similarly, the advantage of $Ni_{[35]}Al_{[32]}Ti_{[2]}Cu_{[3]}$ over a similar configuration where the isolated Ti atom closes the square of NNN bonds between Ti(Al) and the two Cu(Al) atoms. Finally, alloys with N_{Ni} = 34 and N_{Ni} = 33 complete the transition to a regime where dominance of coupling between Cu atoms is the main feature.

V. CONCLUSIONS

The change in site preference in Ni-Al-Ti-Cu alloys was determined experimentally *via* ALCHEMI and theoretically using the BFS method for alloys. In complete agreement with experiment, the BFS calculations also provide an explanation for the observed site distribution of Ti and Cu atoms in the NiAl matrix. A simple approach, based on the definition of local environments, provides additional information regarding the different features in the bonding scheme. It is found that subtle interactions between Ti and Cu atoms, together with their response to the ratio of Ni and Al atoms in the alloy, combine to give Ti the leading role in conserving its behavior when it is the only alloying addition (occupying sites in the Al sublattice) and give Cu a secondary role in individual site preference (Al sites in Ni-rich and Ni sites in Al-rich alloys) as a response to subtle interactions with Ti atoms.

In the range of concentrations studied in the NiAlTiCu system, the behavior extrapolated from the ternary cases (NiAlTi and NiAlCu) coincides with the one observed and calculated for the quaternary alloys. However, additional features regarding the interaction between alloying additions can only be described by a full analysis of the quaternary system, which, in general, are not necessarily a direct combination of the trends observed in the corresponding ternary systems. The formalism introduced in this work thus provides an efficient tool to properly describe complex systems, which could be of extreme use should the interaction between alloying additions result in features not easily predictable from limited experimental evidence.

ACKNOWLEDGMENTS

Fruitful discussions with N. Bozzolo are gratefully acknowledged. We thank B. Good and F. Honecy for their assistance with the Monte Carlo simulations. JEG acknowledges the support of the NASA/OAI Collaborative Fellowship Program and the International Computational Materials Science Consortium. This work was partially funded by the HOTPC project at NASA Glenn Research Center.

REFERENCES

1. Y.L. Hao, D.S. Xu, Y.Y. Cui, R. Yang, and D. Li: *Acta Mater.*, 1999, vol. 47, pp. 1129-39.
2. B.J. Inkson, C.B. Boothroyd, and C.J. Humphreys: *Acta Metall. Mater.*, 1993, vol. 41, pp. 2867-76.
3. Y.G. Li, P.A. Blenkinsop, M.H. Loretto, and N.A. Walker: *Mater. Sci. Technol.*, 1998, vol. 14, pp. 732-37.
4. J. Morgiel: in *Appl. Crystallography Proc. XVII Conf.*, 1998, p. 374.
5. I.M. Anderson, A.J. Duncan, and J. Bentley: *Mater. Res. Soc. Symp. Proc.*, 1995, vol. 364, pp. 443-48.
6. A. Wilson and J. Howe: *Scripta Mater.*, 1999, vol. 41, pp. 327-31.
7. G. Bozzolo, R.D. Noebe, J. Ferrante, and C. Amador: *J. Comput.-Aided Mater. Design*, 1999, vol. 6, pp. 1-32, and references therein.
8. J.C.H. Spence and J. Taftø: *J. Microsc.*, 1983, vol. 130, pp. 147-54.
9. K.M. Krishnan and G. Thomas: *J. Microsc.*, 1984, vol. 136, pp. 97-101.
10. Z. Horita, S. Matsumura, and T. Baba: *Ultramicroscopy*, 1995, vol. 58, pp. 327-35.
11. C.J. Rossouw, C.T. Forwood, M.A. Gibson, and P.R. Miller: *Phil. Mag.*, 1996, vol. A74, pp. 57-76.
12. I.M. Anderson: *Acta Mater.*, 1997, vol. 45, pp. 3897-3909.
13. M.P. Oxley, L.J. Allen, and C.J. Rossouw: *Ultramicroscopy*, 1999, vol. 80, pp. 109-24.
14. S.J. Pennycook: *Ultramicroscopy*, 1988, vol. 26, pp. 239-48.
15. J.L. Defore: *Probability and Statistics for Engineering and the Sciences*. Duxbury Press, New York, NY, 1995.
16. G. Bozzolo, R.D. Noebe, and J. Garces: *Scripta Mater.*, 2000, vol. 42, pp. 403-08.
17. G. Bozzolo, R.D. Noebe, and F. Honecy: *Intermetallics*, 2000, vol. 8, pp. 7-18.
18. G. Bozzolo, J. Khalil, M. Bartow, and R.D. Noebe: *Mater. Res. Soc. Symp. Proc.*, 2001, vol. 646, pp. N6.2.1-N6.2.8.
19. J.R. Smith, T. Perry, A. Banerjea, J. Ferrante, and G. Bozzolo: *Phys. Rev.*, 1991, vol. B44, pp. 6444-65.
20. J.H. Rose, J.R. Smith, and J. Ferrante: *Phys. Rev.*, 1983, vol. B28, pp. 1835-45.
21. O.K. Andersen: *Phys. Rev.*, 1975, vol. B12, pp. 3060-83.
22. G. Bozzolo, C. Amador, J. Ferrante, and R.D. Noebe: *Scripta Metall Mater.*, 1995, vol. 33, pp. 1907-13.